Title	
Author(s)	Samarat, Kaouthar
Citation	
Issue Date	2017-09
Type	Thesis or Dissertation
Text version	ETD
URL	http://hdl.handle.net/10119/14832
Rights	
Description	Supervisor: , ,

Numerical Simulation of Flow and Air-conditioning in Anatomical Realistic Nasal Cavity Model of Chimpanzee

SAMARAT Kaouthar

Japan Advanced Institute of Science and Technology

Doctoral Dissertation

Numerical Simulation of Flow and Air-conditioning in Anatomical Realistic Nasal Cavity Model of Chimpanzee

SAMARAT Kaouthar

Supervisor: KOTANI Kazunori

School of Information Science
Japan Advanced Institute of Science and Technology

September, 2017

ABSTRACT

Traditional research approaches into nasal airways have been critical due to their invasive nature. Recently, with the growth of medical imaging field, it became possible to reconstruct computer models from computed tomography (CT) scans to study the airflow within the nasal passages. Nasal cavity of primates and other animals has been reported in many research works. Lots of the previous studies focused on the nasal airflow but few of them considered the internal nasal air-conditioning phenomena. Furthermore, a proper study of the nasal topology, nasal airflow, and nasal air-conditioning of human's closest being, the chimpanzee, has never been reported.

Nowadays the chimpanzee is regarded as an endangered species which requires specific care and interest. The spread of respiratory infectious diseases is among the crucial dangers to chimpanzees. Addressing the nasal airways, which are the most superior organ of breathing system, is essential for pathologists involved in chimpanzee's medicine. The study of nasal cavity, nasal airflow patterns, and nasal air-conditioning distributions can be a prerequisite to understand chimpanzee's nasal physiology.

The aim of this research is to understand fundamentally the anatomy, inspiratory airflow, and air-conditioning physics of chimpanzee nasal passages. Because the lack of details on the chimpanzee nasal topology, we reconstructed a three-dimensional computer model of the chimpanzee nasal airways based on CT scans.

A detailed description of the nasal anatomy was given based on representative coronal cross-sections of the chimpanzee computer nasal model. An inhalation phase of the airflow was simulated and detailed analysis of the airflow structure within the chimpanzee nasal cavity was reported. The distribution of air-conditioning into the chimpanzee nasal cavity was investigated in distinct sections of the nasal passages, and a comparison of nasal air-conditioning performance between human and chimpanzee was considered.

The results of this study revealed a triangular shaped nasal geometry, as seen from side view, remarkably long and high enough for an efficient air-conditioning. The airflow structure inside the chimpanzee nasal cavity depended on the nasal topology. The inspiratory flow accelerated through the nasal valve, which displayed the smallest cross-sectional area. We noticed the existence of an anterior ventral vortex in the nasopalatine duct region and a dorsal vortex in the olfactory region. We attributed the appearance of both vortices to the increasing of the cross-section in the nasal valve area.

The protrusion of turbinates inside the nasal airways promotes a streamlined airflow in the central nasal passage. The horizontal nostrils and nasopharynx produced a horizontally straight airflow streamlines during inhalation. The computational fluid dynamics model revealed that the inhaled air flows at larger volume and higher rate in the middle airways of the nasal passage, while only small proportion reached the inferior meatus that was created following the protrusion of the inferior turbinate. The superior airways, where the olfactory epithelium is located, passes the least flow at lowest velocity. The minor airflow rate noticed in the dorsal upper part of the nasal cavity reflects a defense strategy that guards the sensitive olfactory nerves to be damaged. The observed vortex in the upper dorsal area of the nasal passage, near the olfactory region, appeared to distract airstreams at high velocity away from the olfactory epithelium.

Simulation of air-conditioning distribution showed that temperature and humidity were gradually adjusted in the middle part of the nasal passages, leading to a conditioned inhaled air at the nasopharynx region. Within the central nasal passages, the air-conditioning was quickly established and adjusted in the regions adjacent to and/or surrounded by the nasal lining such as the meatuses as the heat and water can be immediately exchanged between the tissue layer and the air stream via the epithelial layer, in contrast to the air flowing in the middle passage. No effective air-conditioning was observed within the frontal region of the nasal vestibule. We attributed this fact to the long horizontal nostrils of chimpanzee that are not highly vascular mucous lined airways, consequently cannot provide an ease exchange for heat and water transfer with the inspiratory flow stream. The Chimpanzee's nostrils luminal wall is lined by a squamous layer.

Keywords: Numerical simulation, Chimpanzee nasal cavity, Computational fluid dynamics, Nasal airflow, Nasal air-conditioning.

To my parents, *Hasan* & *Fatima* who
taught me over the years the worth
of labor and persistence, values
that propped me to get to
this point.

ACKNOWLEDGEMENTS

<div align="right">

SAMARAT Kaouthar
September, 2017

</div>

TABLE OF CONTENTS

LIST OF TABLES

LIST OF FIGURES

CHAPTER I

INTRODUCTION

1.1   Motivation

Chimpanzees are colloquially named chimps. Research by Minkel in 2006 found 94% of DNA commonality between human beings and chimpanzees (Minkel, 2006). Such close kinship between human and chimpanzee may provide exclusive understanding of human biology through chimpanzee's studies (Tarjei, et al., 2005).

Decades ago, there were probably millions of chimpanzees living throughout tropical Africa. Nowadays, chimpanzees are regarded as an endangered species, and their population is continuously declining.

Disease is considered among the major dangers threatening chimpanzees. The usage of chimpanzee in experimentation is rising (Tarijei, et al., 2005; Gagneux, et al., 2005), and the increased dealings with humans has carried the menace of ailments that could be minor in human being but fatal to chimpanzee (House, et al., 1966).

Usually, chimpanzee's medical care presumes the identity of its physiology and pathology with human. Although humans and chimpanzees are biologically akin, they may be obviously different in their vulnerability to diseases (Gagneux, et al., 2005).

After one year observation study of chimpanzees, Kaur and coworkers (2008) stated that endangered chimps becoming sick from respiratory viral infectious diseases transmitted from research teams and eco-tourists (Kaur and Singh, 2008).

The respiratory tract is largely reported in chimpanzees' disease. Many research works investigated respiratory system diseases related to primates in general (Lapin et al., 1963; Fiennes et al., 1972a; Fiennes et al., 1972b; Martin, 1978; Wallach et al., 1983; Lowenstine, 2003). Table A.1 reviews the range of respiratory disease in chimpanzee.

Respiratory system structure is complicated. It meets multiple physiological tasks such as the contact between air and blood, which likely carries with it an exposure to damaging agents. An understanding of respiratory tract and reported respiratory problems in chimpanzee, as well as associated diagnostic approaches and pathology, may widely improve chimps' clinical management.

The nose is the most superior organ of the breathing system. Its function comprises air exchange, air-conditioning, filtration, vocalization, and sense of smell (Hornung et al., 1981).

Our limited knowledge may restrain our concern about increasing medicine understanding and scientific challenges specific to endangered chimp. Familiarity with chimpanzee nasal topology, airflow patterns, and air-conditioning structures is a source of knowledge to understand chimp's nasal physiology and pathology. This fact could potentially contribute in accumulating standardized biological information on healthy chimpanzees, and so increasing the ability to care for them. It would also support scientists interested in comparative biomedicine filed.

1.2 Objectives

This research work aimed to develop a CFD approach in order to present details about anatomy, airflow structures, and air-conditioning patterns in a chimpanzee nasal cavity. The focus may be categorized into three parts: (i) nasal anatomy (ii) analysis of airflow patterns of an inspiratory phase under physiological flow rate and (iii) visualization of air-conditioning distributions through the nasal airways.

The CFD approach aimed at:

  - Acquiring a detailed understanding of chimpanzee's nasal airways topology. A computer nasal geometry was modeled from computed tomography (CT) scans.

  - Visualizing inhaled airflow patterns of chimpanzee nasal topology using computational fluid dynamics (CFD) approach.

  - Providing an overview of the air-conditioning distribution inside the nasal cavity of chimpanzee, and discussing the role of anatomical features of the nasal topology in heat and water transfer.

  - Comparing the nasal air-conditioning performance of chimpanzee and human.

The results of this study may confirm the changeability between nasal geometries of different species and determine how airflow patterns would dependently affected.

1.3 Methodology

The difficulties involved with experiments led into investigation of the nasal airflow field using computational fluid dynamics (CFD) approach. CFD enables comprehensive measurements of airflow parameters without any intervention risk for the subject. To begin the CFD process, a

geometrical model of the nasal cavity is initially required. This means either assuming a simplified geometry or obtaining medical scans (CT or MRI) in their electronic format so that they can be uploaded into a computer. The reconstruction and determination of the nasal geometry in this study was done by CT scans. The geometric model is then divided into smaller sections (cells) to create a mesh. The flow equations are then solved numerically for each and every cell to give information about the flow parameters within the entire nasal model.

This research work intended to build an accurate realistic chimpanzee nasal cavity from CT scans. Modelling of the 3D geometry was accomplished using CAD (Computer-Aided Design) software. Compared to cast models, biomedical scans are much more accurate in offering detailed data leading to realistic airways geometry. This research work attempted to find out how the airflow patterns, its velocity, and the air-conditioning distributions are structured inside the chimpanzee nasal cavity. The nasal airflow patterns and the air-conditioning distributions were generated using CFD approach.

1.4   Dissertation structure

The motivation to conduct this research work, the objective, and the outline of the dissertation are presented in Chapter one.

Chapter two reviews previous studies of nasal cavity in animals, three-dimensional nasal reconstruction, and computational studies of nasal airflow.

Third chapter reports the process to build the nasal topology. The computational model includes the stages of image processing (sub-image extractions from CT scans), surface generation, and volume mesh construction.

Fundamental concepts related to the mathematical and numerical methodologies for fluid flow are discussed in chapter four. The governing equations that are solved are described.

Chapter five explores the anatomical aspects of the chimpanzee nasal topology. These results were discussed and compared to available data of human and rhesus monkey nasal airways.

Chapter six analysis the airflow structure and air-conditioning distributions. Patterns thru different areas of the nasal topology counting the nasal valve and meatuses are described. The heat and water transfer capability of the chimpanzee nasal cavity is also discussed. The temperature and humidity distributions reflected the effect of the conchae and their role in conditioning the inspiratory.

Chapter seven focused on comparing air-conditioning efficiency inside the nasal cavities of human and chimpanzee. Specifically, hot-humid and cold-dry inhaled air cases were computed. The influence of the inhaled air parameters on the airflow patterns was highlighted.

Finally, we conclude this dissertation in chapter eight.

CHAPTER II

LITERATURE REVIEW

Because the complex geometry of the nasal cavity, in vivo experimentations of the nasal airflow is problematic. Previous experimental work on animals' nasal cavities has been done on cat (Eccles et al., 1974), dog (Webber et al., 1987), pig (Eccles, 1978), rat (Bojsen-Moller et al., 1971), and ferret (Reo et al., 1992). Eccles et al., (1981) studied the autonomic innervation in animals' nose (Eccles et al., 1981). Various studies investigated the morphometry of nasal airways for different Mammalia such as the beagle dog (Schreider et al., 1981), rat (Schreider et al., 1981; Gross et al., 1982; Patra et al., 1987; Kimbell et al., 1997), monkey (Schreider et al., 1981; Yeh et al., 1997; Kepler et al., 1998; Harris et al., 2003), mouse (Gross et al., 1982), guinea pig (Schreider, 1983), and human (Yeh, et al., 1997; Menache, et al., 1997; Subramaniam, et al., 1998) using sections of nasal cavity casts, slices' series from fixed tissue of the nasal cavity, or medical imaging scans (either CT or MRI).

One promising field is based on dynamics assessment using the nasal airflow. This has been brought to attention since the nasal physiological function is strongly dependent on the nasal airflow dynamics. Most research methods recorded nasal airflow indirectly such as using a passive airflow through the nose to determine pressure changes.

Experiments to visualize nasal airflow have been conducted for human (Paulsen, 1882; Proetz, 1951, 1953; Swift, et al., 1977; Hornung, et al., 1987; Simmen, et al., 1999), cat (Dawes, 1952),

dog (Dawes, 1952; Becker, et al., 1957), rabbit (Dawes, 1952; Corley, et al., 2009), baboon (Patra, et al., 1986), monkey (Morgan, et al., 1990, 1991), and rat (Morgan, et al., 1990, 1991). To visualize the airflow patterns of inhalation and exhalation phases, Dawes (1952) used the smoke associated with sagittal sections of dog nasal airways (Dawes, 1952). Other researches (Becker, et al., 1957) used aerosols and particles' deposition to visualize nasal airflow patterns. Water-dye visualization techniques (Swift, et al., 1977; Morgan, et al., 1990, 1991) was the most encouraging at showing the airflow patterns inside the nasal cavity.

Experiments of nasal airflow quantitative measurements have been done for human (Hopkins, et al., 2000; Swift, et al., 1977; Hahn, et al., 1993; Kelley, et al., 2000) and baboon (Patra, et al., 1986). Other researchers investigated the flow measurement using MRI technique (Elkins, et al., 2003; Taylor, et al., 2004; Marshall, et al., 2004; Elkins, et al., 2007; Vennemann, et al., 2007; Bonn, et al., 2008).

Investigations of main primate taxa (Wen, 1930; Schultz, 1935) contributed to the knowledge of nose structure in primates. The comparative study of the nasal cartilages in primates by Wen (Wen, 1930) has shown the importance of these structures for the configuration of the outer nose which differ among the group of primates. Later on, Hofer (Hofer, 1976) focused on the external nasal structure.

Most early studies of primates' nasal structure were carried out on fetal stages using serial sections, which cartilages normally disappear at various postnatal stages. As per older animals which cannot be dissected, their gross nasal anatomy are still unknown.

Albeit the research efforts, the dynamics of the nasal airflow in animals is still considered a new topic in the scale of scientific research. There are still many uncertainties even in some of the most basic flow principles, such as the nature and the main path of the nasal airflow as visualization and measurement of nasal airflow remain challenging due to the geometrical complexity and the

reduced nasal airways size, so accuracy of experimental data remains limited. On the other hand, discrepancies in the nasal airflow fields when investigated by CFD techniques may arise due to different numerical methods and flow assumptions.

Due to software and hardware development and their recent availability, CFD approach is currently used to study living organs including the nasal cavity. Over few decades, investigators relied on geometrically simplified models for their CFD computations. They designed their models with the aid of graphics software by using data from literature (Weibel, 1963) to estimate the dimensions of their models (geometrical shape, perimeter, cross-sectional area, etc.). Nowadays, with the advancement in biomedical imaging field and computer technological development, researchers became able to develop more geometrically realistic models.

Biomedical imaging such as CT and MRI scans together with 3-dimensional (3D) modelling software endorsed the reconstruction of computer models of the nasal cavity for analysis. By generating different nasal computational models, CFD simulations of inhalation (Minard, et al., 2006; Timchalk, et al., 2001; Kimbell, et al., 1993, 2001; Kepler, et al., 1998; Subramaniam, et al., 1998; Kimbell, et al., 1997), respiration (Lindemann, et al., 2004), and sense of smell (Keyhani, et al., 1995, 1997) have been done. Reconstruction of airways geometry may be done with accuracy comparing to cast models or even cadavers examination. Other researchers used the reconstructed models to create their experimental biological models of intricate geometry with more details (Stitzel, et al., 2003; Hopkins, et al., 2000).

Using CFD technology, various research works reported nasal airflow patterns of human, monkey, and rat in studies of inspiration toxicology (Minard, et al., 2006; Kimbell, et al., 1993, 1997, 2001; Subramaniam, et al., 1998; Kepler, et al., 1998), olfaction (Tang, et al., 2007; Zhao, et al., 2004, 2006; Keyhani, et al., 1995, 1997), and air-conditioning (Nishimura et al., 2016; Mori, et al., 2015; Hanida, et al., 2013; Kumahata, et al., 2010; Lindemann, et al., 2004, 2006; Pless, et al., 2004).

MODELLING OF CHIMPANZEE NASAL GEOMETRY

3.1 Medical image processes

The nasal cavity has a complex geometry which makes the use of Computer Aided Drafting (CAD) unpractical to design its computer model. Recently, the growing concern toward biomedical research field and technology advancement have lead up to develop software useful for creating 3D models from medical images. Modern modalities offer digital data more compatible for three-dimensional reconstruction and computational analysis (Timchalk et al., 2001; Minard et al., 2006) than anatomic sketch provided by early sectioning techniques (Kimbell et al., 1993, 1997, 2001).

To develop a computer model of a nasal passage, someone needs first to acquire the anatomical data of the test subject. Medical imaging data provide voxels (volume elements) of different structures associated with their tissues, that can be distinguished based on threshold of greyscale or brightness. Currently favored medical imaging techniques include CT and MRI.

3.1.1 Computed tomography (CT)

Developed by Sir Godfrey in 1972 (Richmond, 2004). Computed Tomography (CT) is a medical imaging medium that assists doctors in diagnosing pathology by allowing the scan of multiple cross-sections of internal organs and structures of subjects in order to view them. Dissimilar tissues in patient's body possess various X-ray absorption and transmissivity levels. CT machine measures

radiation beams by applying an instrument of great sensitivity, and thus obtains measurement data able to be inputted and processed into a computer.

CT scanning consists of X-ray beams of radiation that focuses onto a subject in order to define its structure and internal shape by generating cross-sectional images. X-rays released by a CT machine scan a definite level of thickness of subject's internal organ and are then detected by a probe. The photoelectric data are converted into electrical signals, and then, through a digital converter, are converted into numbers which may be input to the computer (Figure 3.1). The scanned data undertake a calculation into the computer to get each individual information of X-rays attenuation and/or absorption coefficients and arrange them into a digital matrix. CT is largely used in medical settings due to its diagnostic worth and relatively low-priced apparatus. However, CT scanning exposes subjects to relatively high ionizing radiation levels and has qualitative diagnosis limitations compared to other imaging mediums.

(a)   (b)

Figure 3.1. *(a)* Computed tomography scans (sliced images). *(b)* Modern CT scanner.

(https://upload.wikimedia.org/wikipedia/commons/3/35/113abcd_Medical_Imaging_Techniques.jpg)

3.1.2 Comparison between CT and MRI

Both CT and MRI images provide 3D volumetric data sets. Additionally, CT scanning generates voxel greyscale values' matrix into which the voxel tissue's of CT number to be arranged. As dissimilar tissues present dissimilar characteristics of attenuation and/or absorption, subsequent sliced image differentiates dissimilar tissues by greyscale. This permits a good detection of bone structures. This fact offers CT an advantage over MRI. In regard to the nasal airways, MRI differentiates well structures of mucosa, though the location of turbinate cartilage should be deduced from its mucosal neighboring, because bone actual structures can be invisible. During their comparative study of MRI to CT scans done on paranasal sinuses and nasal cavities of mesaticephalic dogs, De Rycke and co-workers (2003) noticed the efficiency of MRI over CT scans in soft-tissue structure resolution (De Rycke, et al., 2003). Zinreich and co-workers (1988) reported that MRI method is less effective in modeling nasal airways geometry (Zinreich et al. 1988). In this research work both methods can provide the necessary data since our focus is only on the structure of bone without need for high-resolution of the soft tissue.

Figure 3.2 provides a comparison example of MRI to CT scans.
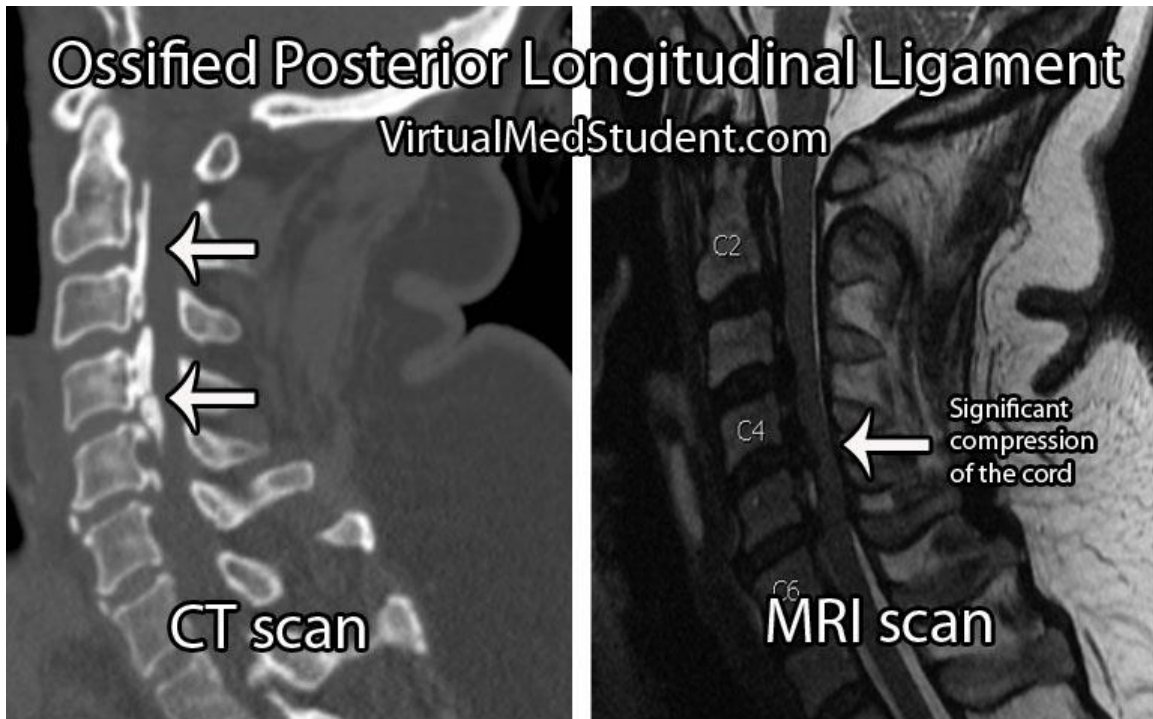
Figure 3.2 CT vs MRI scans

(http://www.virtualmedstudent.com/images/ossified_posterior_longitudinal_ligament_MRI_and_CT.jpg)

3.2 Computer modelling of the chimpanzee nasal passage

Prior to the creation of a CFD model, chain of procedures associated with the design and development of the model should be achieved. The process of making a computer model may be done thru five steps: (i) Acquisition of anatomical data; (ii) extraction; (iii) reconstruction of a closed surface; (iv) surface smoothing; (v) and generation of volume mesh. Figure 3.3 illustrates the process from converting the raw CT anatomical data till the generation of three-dimensional mesh.

Anatomical data (aquisition of raw 2D CT slices from the test subject which supplies a launching for the investigation)

Extraction (sub-images creation)

Surface reconstruction (closed surface defining the nasal shape)

Smoothing (surface refinement)

Mesh generation (three-dimensional surface model)
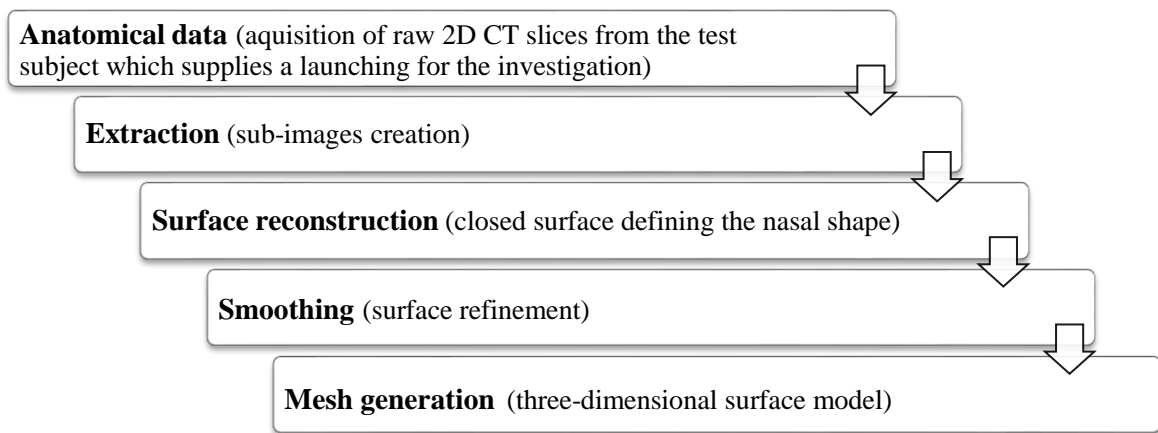
Figure 3.3 Three-dimensional surface generation methodology

3.2.1 Anatomical data

The CT scanning used in this study consisted of 401 slices, spanned from mouth tip to just anterior to larynx, of the head of an adult female chimpanzee (estimated age: 35-year-old; weight: 44.1 kg), Pan troglodytes reared at the Primate Research Institute, Kyoto University (KUPRI), Inuyama, Japan (Matsuzawa, et al., 2006). Each slice was composed of 512 x 512 pixels in the DICOM format. Scans resolution was 0.351 mm/pixel and scans pitch was 0.5 mm/slice. The scans were performed in three different axial positions. The CT scans are available on the digital morphology museum (DMM) database (http://dmm.pri.kyoto-u.ac.jp), of the Primate Research Institute, Kyoto University, Inuyama, Japan (CT scans id: PRICT #467 and 468).
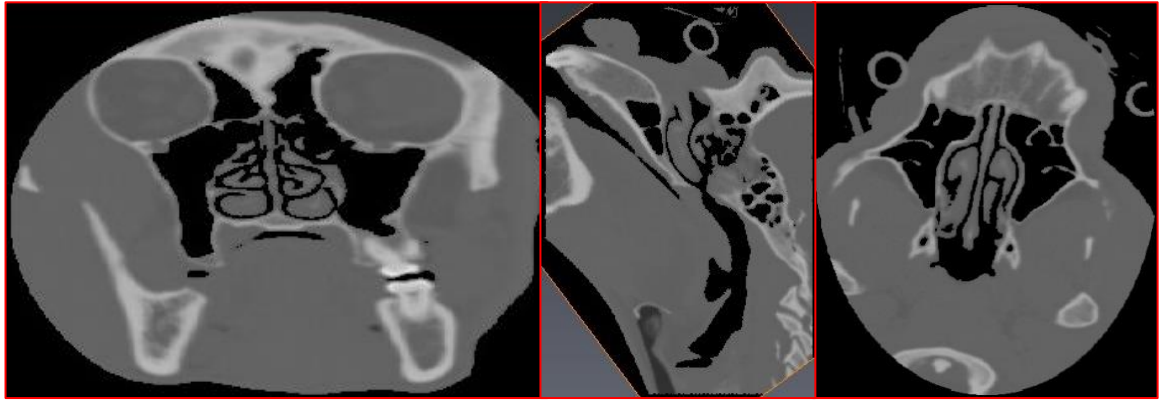
(a) Plane *xy*   (c) Plane *yz*   (b) Plane *xz*

Figure 3.4 Slice samples of CT scans of the chimpanzee head: *(a)* Plane *xy*, *(b)* Plane *yz*, *(c)* Plane *xz*.

3.2.2 Extraction: Sub-image creation

CT scans data consisted of serial coronal sections containing a threshold of greyscale to distinguish different bony structures (Figure A.2). Avizo (Visualization Science Group) software for visualizing CT scans, is an interface between scanned data, STL file format, and CFD analysis. Anatomical data consisted of cross sections of the chimp's head spanned from the mouth tip to just anterior of the larynx. Considering constraints of resources and time, we limited our interest to the nasal cavity only. The black area represents the airways, was extracted (Figure A.3) based on brightness' threshold using Avizo 7 software (Figure 3.5). This extraction leads to a sub-image creation necessary for (a) reducing the computational cost and (b) removing the noise (undesirable regions) out the airways. Figure 3.5 displays a raw CT scan with its corresponding extracted sub-image.

Figure 3.5 Comparison between raw and processed data of a same CT scan: One sliced image displaying a coronal cross section of the chimpanzee head (left); Extraction of a sub-image showing the nasal passage topology (right). Total number of CT scans was 401 slices.

3.2.3 Surface reconstruction

To generate a 3D surface following the sub-images creation, the extracted subset of CT scans was exported and the voxel data was converted to STereo Lithography (STL) file format into Avizo. The obtained data of the STL file were read into the computer program and a surface was generated through image reconstruction saved in STL format. The file (Figure 3.6) will then be exported to a suitable software for smoothing.
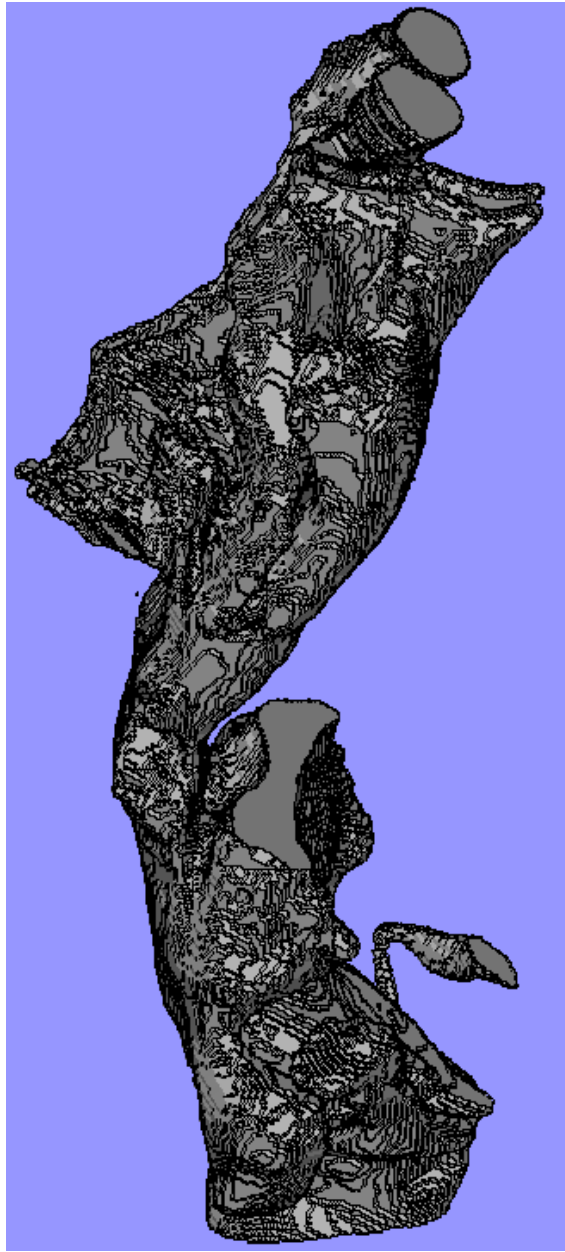
Figure 3.6: Reconstructed surface generated from the extracted subset of CT scans.

3.2.4 Smoothing

The nasal airways model of the generated surface should exhibit some irregularities. To avoid distortion in the flow filed values, the reconstructed surface (Figure 3.8a) was refined by performing global and local smoothing in order to remove warping and alleviate the in-built discontinuities generated by the numerous slices and resulting discrepancies. We used Magics 9.5 software (Materialize Inc., Leuven, Belgium) to modify the above data into a smooth surface (Figure 3.8b). The smoothing used in this research work consisted of shifting the vertices of triangulated surfaces in a manner to become more refined. The number of global smoothing is decided by the user. To optimize between keeping the initial geometry and eliminating irregularities, the global smoothing was applied only twice. Local smoothing is a manual process which is a repetitive and time consuming exercise. Several different-sized/shaped holes may appear randomly which necessitates individual manual removal by editing each nearby area while identifying local odd shaped triangles to delete them in order to smoothen the global surface. Holes can be filled using either curvature filling or flat filling techniques. Because of the complexity and highly curved shape of the nasal geometry, curvature filling was perfectly suited since it blended the hole to fit the adjacent area. The flat filling was adequate in case of very small holes. The smoothing was applied in the 3-axial directions. At first, necessary local smoothing on each single irregularity throughout the whole external surface was performed. Then, a manual smoothing in the internal side of the closed airways surface was done to remove unrelated sub-regions, recognized by their shape singularities relative to the whole topology. To ensure maintaining the fundamental geometry as accurate and reliable as possible, amendment of the surface have to be kept to a least possible.

The refined surface was then exported from Magics and opened in Avizo (Figure 3.8b). This transfer into Avizo was required in order to specify the locations of nostrils and nasopharynx. This block data need a manual removal to outline nostrils and nasopharyngeal regions (Figure 3.7).
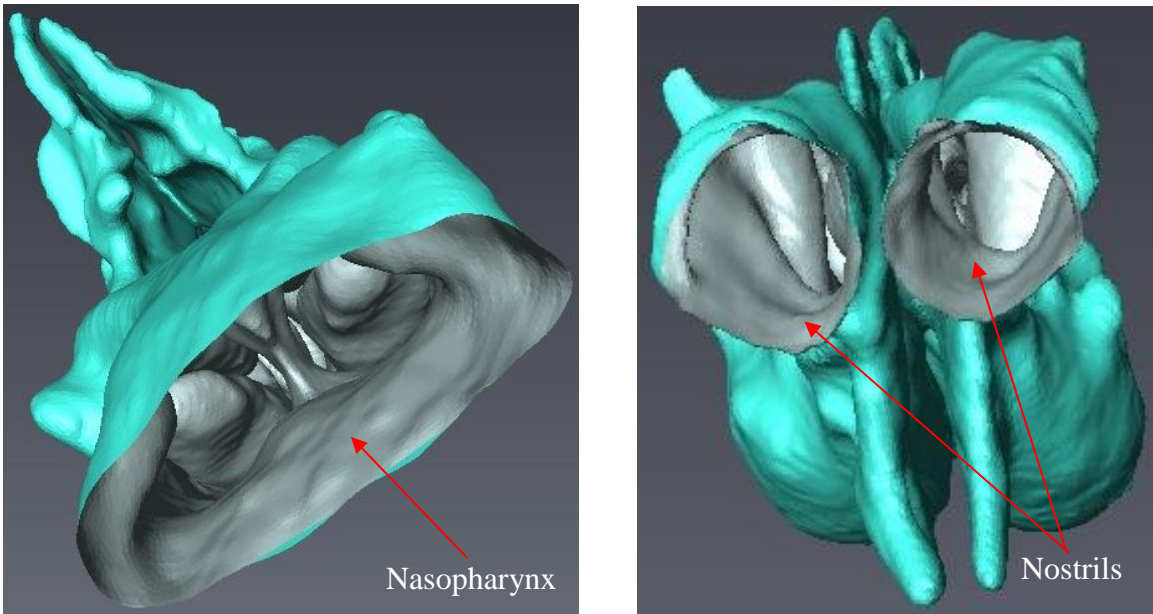
Figure 3.7 Selection of block data that needs manual removal to outline the shapes of nostrils and nasopharynx.

Neighboring the main model, minor isolated data points may exist. This undesirable 'noise' needed to be manually removed since they were not parts of the actual geometry. The deletion of unwanted data made the working process more efficient by optimizing computational resources such as overall speed, memory, and power. The file (Figure 3.8c) is then exported to the suitable CFD software in order to define the domain of airflow and generate the volume mesh.
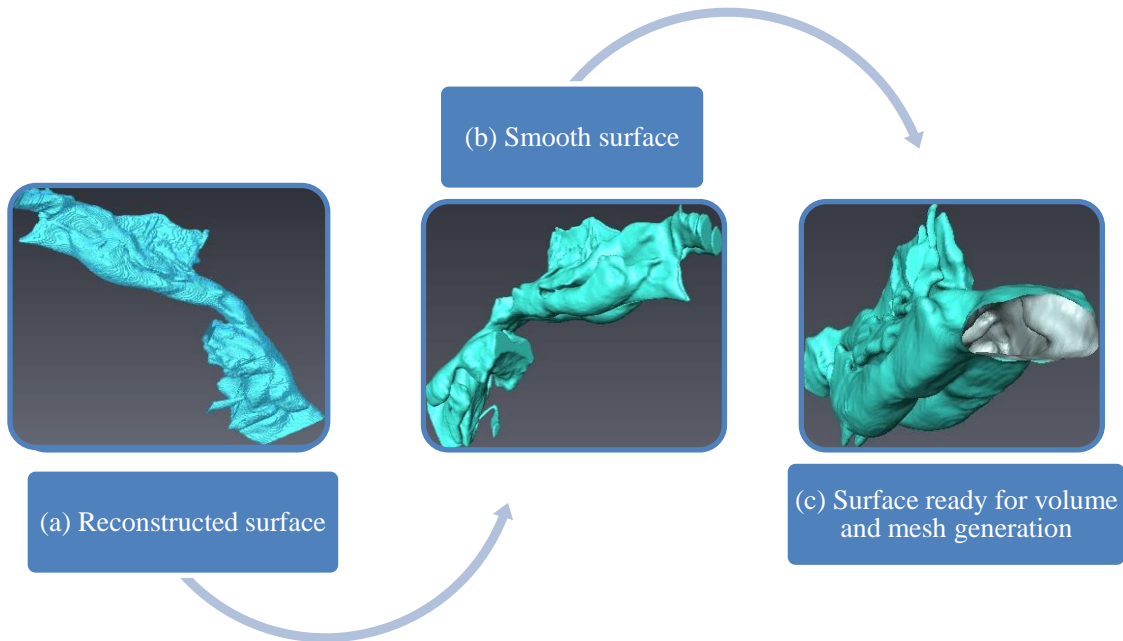
Figure 3.8 Surface ready for volume mesh generation.

3.3 Development of the CFD model

The creation of the mesh is a major operation in achieving accurate computational results during CFD simulations. In this research work, we used GAMBIT (ANSYS) software for mesh generation. The reconstructed surface was exported from Avizo as STL format file, to be imported into GAMBIT which detected the generated surfaces as faces.

The advantages of a structured mesh are the reduced memory needed for computation and better convergence solution, however impractical in case of complex geometry such as the nasal cavity. An unstructured grid has the advantage for complicated shapes of using tetrahedron cells that may be clustered under control in the flow domain where it is needed. Whereas structured mesh forcibly places hexahedron elements in regions where they are not wanted. The unstructured grid might suit complex topologies, requiring considerably more computational resources, as neighboring nodes to each individual node increase. Yet, tetrahedron cells can never be aligned to the direction of the flow. This problem may impede convergence. Increasing mesh resolution and choosing

discretization schemes of higher order are techniques that minimize the possibility of numerical diffusion.

3.3.1 CFD model

The smoothed data was imported into Gambit 2.4 (ANSYS Inc., Canonsburg, PA, USA) under STL format. The reconstructed surface was detected as faces. The meshing approach started with setting basics for the face mesh and then generating volume cells founded on the face mesh (Figure 3.9). For the complex geometry of the chimpanzee nasal cavity, an unstructured tetrahedron grdid for CFD analysis was generated with a grid step of 0.3. The mesh contained about 3.7×10^6 tetrahedron cells, 7.6×10^6 triangles, and 7.4×10^5 non duplicated nodes. Its surface area and total volume were 185.41 cm^2 and 41.64 cm^3, respectively.
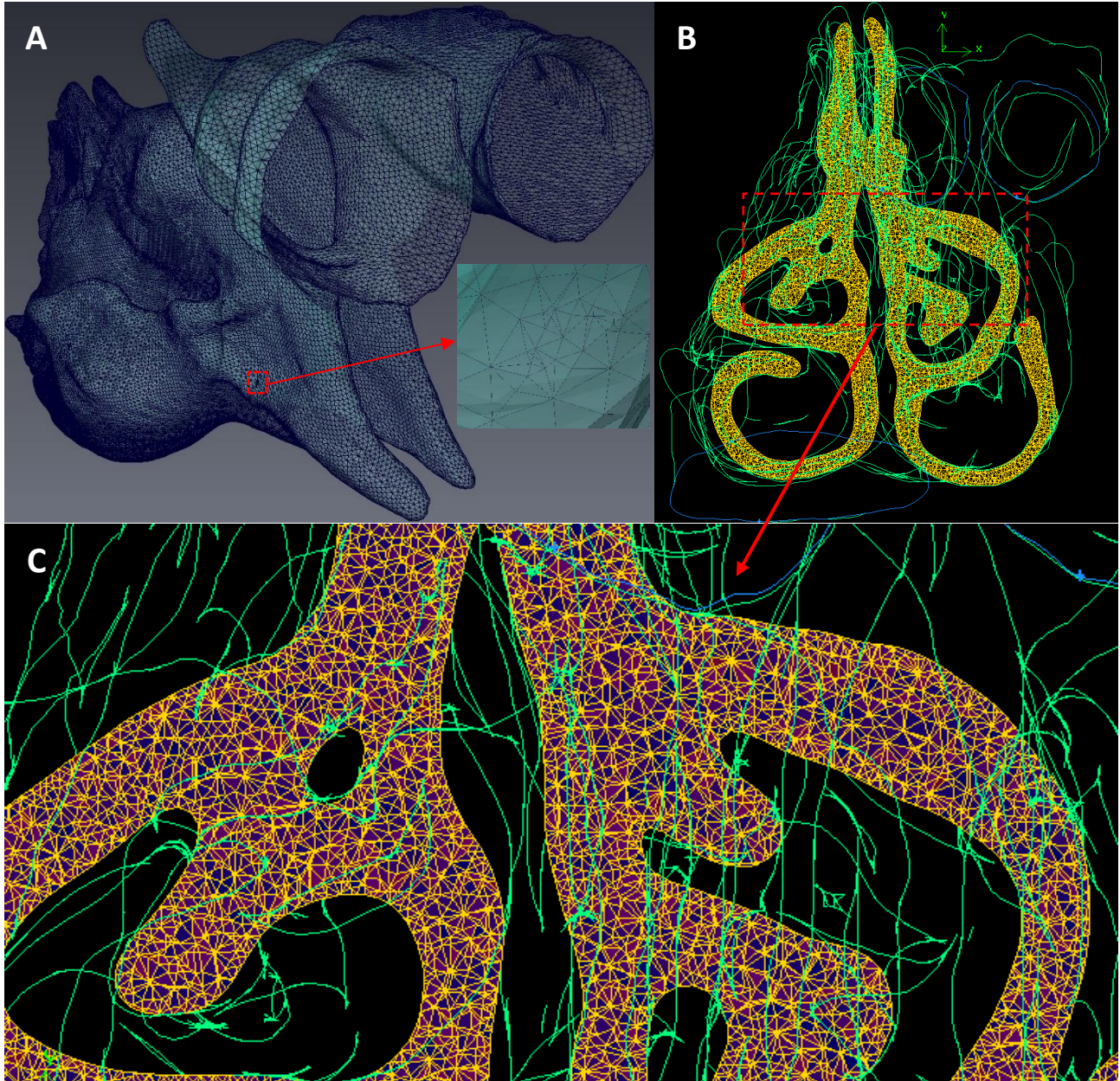
Figure 3.9 Computer model of the chimpanzee nasal cavity: Face meshing of the generated surface (A); Coronal cross-section of the computational volume mesh (B); Zoom showing unstructured tetrahedron cells (C).

CHAPTER IV

NUMERICAL METHOD

4.1 Introduction

Chapter four is about the used mathematical equations for numerical simulations. The laminar state model was used to simulate an inhalation case at rest physiological rate. The details of setting the boundary conditions are not discussed in this chapter. They are instead described in chapter 6.

4.2 Fluid flow general governing equations

Computational fluid dynamics basically use the general Navier-Stokes equation that governs the flow and heat transfer within a fluid domain. General Navier-Stokes equation includes an equation of continuity, three equations of momentum, and an equation of energy.

Airflow inside the nasal cavity is regarded as a continuum. Its behavior can be described using its properties for example density, velocity, and their derivative with respect to time. Moreover, it is considered as incompressible fluid.

Defining a fluid property as ϕ, the governing equations of incompressible fluid flow might be represented by the equation of transport (Eq. 4.1) under its generic form:

$$\underbrace{\frac{\partial \emptyset}{\partial t}}_{\text{local acceleration}} + \underbrace{\frac{\partial(u\emptyset)}{\partial x} + \frac{\partial(v\emptyset)}{\partial y} + \frac{\partial(w\emptyset)}{\partial z}}_{\text{advection}} = \underbrace{\frac{\partial}{\partial x}\left[\Gamma\frac{\partial \emptyset}{\partial x}\right] + \frac{\partial}{\partial y}\left[\Gamma\frac{\partial \emptyset}{\partial y}\right] + \frac{\partial}{\partial z}\left[\Gamma\frac{\partial \emptyset}{\partial z}\right]}_{\text{diffusion}} + \underbrace{S_\emptyset}_{\text{source term}} \quad (4.1)$$

t denotes time; u, v and w denote the components of velocity, Γ denotes diffusion coefficient, and

S_ϕ represents a source term.

Equation 4.1 is the start-up of finite difference and finite volume methods. By affecting the values

of 1, u, v, w and T, to ϕ, and setting appropriately the diffusion coefficient Γ and the source term

S_ϕ, we get the partial differential equations of mass conservation, momentum conservation, and

energy as presented in the following table.

Table 4.1 The Navier-Stokes equation of an incompressible fluid flow

Mass conservation

$$\frac{\partial u}{\partial x} + \frac{\partial v}{\partial y} + \frac{\partial w}{\partial z} = 0 \qquad (4.2)$$

Momentum conservation

$$\frac{\partial u}{\partial t} + \frac{\partial(uu)}{\partial x} + \frac{\partial(uu)}{\partial x} + \frac{\partial(uu)}{\partial x} = -\frac{1}{\rho}\frac{\partial p}{\partial x} + \frac{\partial}{\partial x}\left[\nu\frac{\partial u}{\partial x}\right] + \frac{\partial}{\partial x}\left[\nu\frac{\partial u}{\partial x}\right] + \frac{\partial}{\partial x}\left[\nu\frac{\partial u}{\partial x}\right] + S_u \qquad (4.3)$$

$$\frac{\partial v}{\partial t} + \frac{\partial(uv)}{\partial x} + \frac{\partial(vv)}{\partial y} + \frac{\partial(wv)}{\partial z} = -\frac{1}{\rho}\frac{\partial p}{\partial y} + \frac{\partial}{\partial x}\left[\nu\frac{\partial v}{\partial x}\right] + \frac{\partial}{\partial y}\left[\nu\frac{\partial v}{\partial y}\right] + \frac{\partial}{\partial z}\left[\nu\frac{\partial v}{\partial z}\right] + S_v \qquad (4.4)$$

$$\frac{\partial w}{\partial t} + \frac{\partial(uw)}{\partial x} + \frac{\partial(vw)}{\partial y} + \frac{\partial(ww)}{\partial z} = -\frac{1}{\rho}\frac{\partial p}{\partial z} + \frac{\partial}{\partial x}\left[\nu\frac{\partial w}{\partial x}\right] + \frac{\partial}{\partial y}\left[\nu\frac{\partial w}{\partial y}\right] + \frac{\partial}{\partial z}\left[\nu\frac{\partial w}{\partial z}\right] + S_w \qquad (4.5)$$

Energy equation

$$\frac{\partial T}{\partial t} + \frac{\partial(uT)}{\partial x} + \frac{\partial(vT)}{\partial y} + \frac{\partial(wT)}{\partial z} = \frac{\partial}{\partial x}\left[\left(\frac{\nu}{Pr}\right)\frac{\partial T}{\partial x}\right] + \frac{\partial}{\partial y}\left[\left(\frac{\nu}{Pr}\right)\frac{\partial T}{\partial y}\right] + \frac{\partial}{\partial z}\left[\left(\frac{\nu}{Pr}\right)\frac{\partial T}{\partial z}\right] + S_T \qquad (4.6)$$

4.3 Numerical solver procedure

A CFD solution process includes three phases: (i) pre-processor, (ii) solver, and (iii) post-processing.

The pre-processor phase consists of defining the geometry to be analyzed, the domain of computation, and the properties of fluid. At this step, the type of analysis should be decided as steady, transient, or unsteady flow, and whether its state is laminar or turbulent. The fluid flow

behavior is important for defining the appropriate boundary conditions of the flow domain. The chosen settings need to imitate the real behavior of the fluid.

The second phase of a CFD simulation is the settings of the numerical method. The determination of an adequate computational technique for the solution leads to reliable results. These techniques include discretization scheme, pressure-velocity coupling scheme, and convergence criteria. We choose FLUENT segregated solver to solve Navier-Stokes equations. Figure 4.1 shows solver's flow chart.

Last stage is the Post-processing, which consists of converting raw data into significant outcomes. CFD offers the possibility to produce precise detailed data and colorful illustrations including streamline, contour, and vector plots.

```
        ┌─────────────────────┐
        │        Start        │
        └─────────────────────┘
                   │
                   ▼
        ┌─────────────────────────────────┐
        │     Updating fluid properties   │
        └─────────────────────────────────┘
                   │
                   ▼
        ┌─────────────────────────────────┐
        │ Resolve equation of momentum (u, v, w) │
        └─────────────────────────────────┘
                   │
                   ▼
        ┌─────────────────────────────────┐
        │   Resolve continuum equation (p)   │
        └─────────────────────────────────┘
                   │
                   ▼
        ┌─────────────────────────────────┐
        │ Solve energy equation (Temperature T) │
        └─────────────────────────────────┘
                   │
                   ▼
        ┌─────────────────────────────────┐
        │ Solve transport equation (Mass fraction of water F) │
        └─────────────────────────────────┘
                   │
                   ▼
      No  ◇───────────────────────◇
          ◇       Converged       ◇
           ◇─────────────────────◇
                   │ Yes
                   ▼
        ┌─────────────────────┐
        │         End         │
        └─────────────────────┘
```
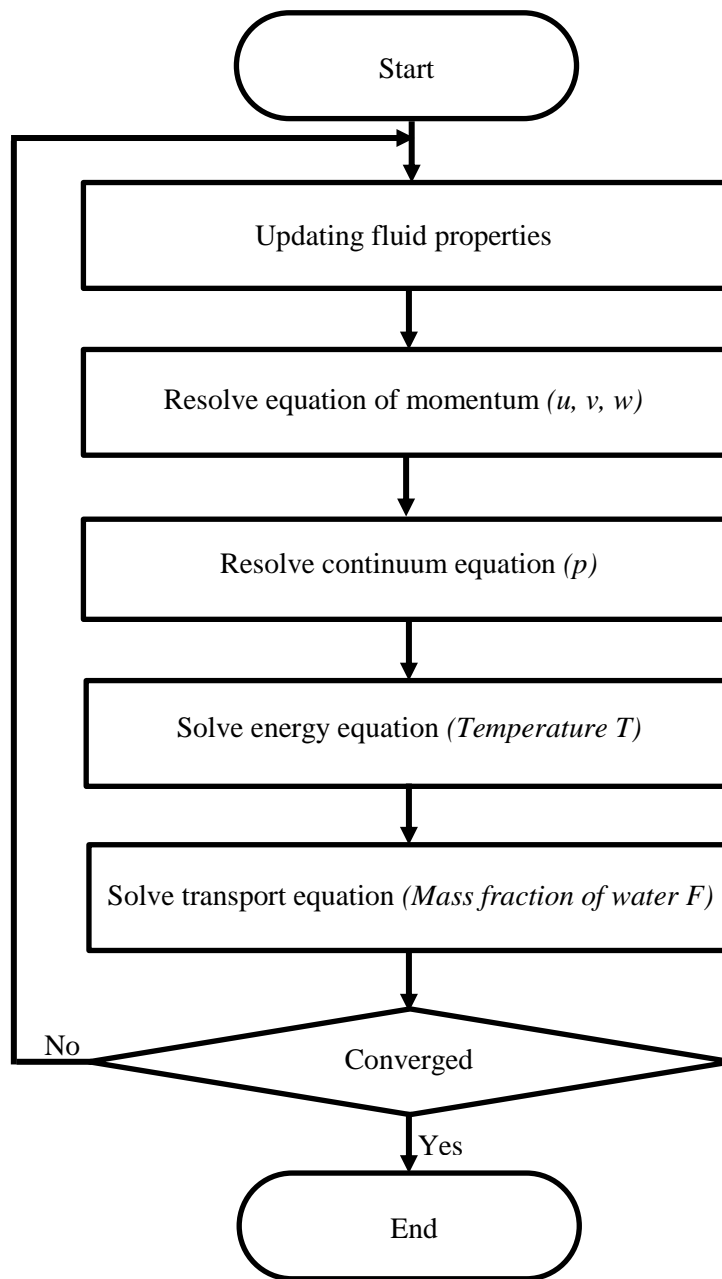
Figure 4.1 Flow chart of the segregated solver

4.4 Fluid flow discretization

There are few different discretization schemes of a fluid flow that may be classified according to the accuracy they may offer. The minimum accurate one is the first order scheme, subsequently subject to producing unreliable outcomes. Second order upwind scheme reduces some of the faults generated in first order scheme. Influence of the grid refinement is further significant with a first order scheme than a second order scheme. The third order (QUICK) scheme offers accuracy for greater choice of flows in comparison to the first order and Upwind schemes.

For incompressible flows, an iterative method for pressure-velocity coupling named SIMPLE scheme (Patankar, 1980) is widely used and may be found in almost all CFD codes.

We used the QUICK scheme (Leonard, et al., 1990) to solve the Navier-Stokes equation where the SIMPLE algorithm (Vandoormaal, et al., 1984) was employed for the calculation of the pressure and velocity.

CHAPTER V

NASAL ANATOMY OF CHIMPANZEE

5.1 Chimpanzee nasal topology

The images taken by CT scanning are reconstructed and derived to form a three-dimensional geometry for simulating nasal airflow in the later stage. Several types of software have been involved. The following results represent the most detailed anatomic data of a chimpanzee nasal passages. Indeed, accurate experimental determination of nasal airways details is generally problematic because of the narrow dimensions of the nasal passages and the disruptive effect of manipulation tools.

Studying a range of chimpanzee specimens at this level of detail is not presently practical and is well beyond our present scope. Instead, details of some anatomic regions within a typical chimpanzee nasal topology are given. Following the results presented here, a discussion and comparison of available data from human and limited data from the rhesus monkey (Kepler, et al., 1998; Morgan, et al., 1991), with our computer model of chimpanzee nasal topology is given in the subsequent section.
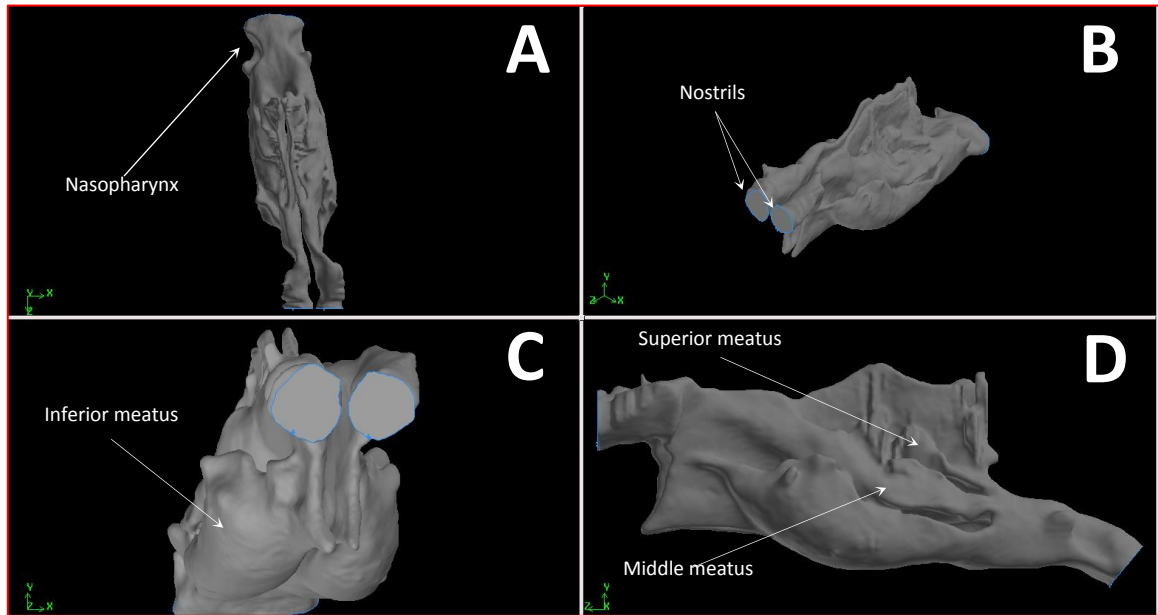
Figure 5.1 Model of nasal passages anatomy: *(A)* Top view, *(B)* 3D view, *(C)* Front view, *(D)* Side view. The anatomy was reconstructed from 401 head CT slices of a healthy 35-year-old female chimpanzee weighing 44.1 Kg. The nasal cavity is sectioned by thin, curved, bony shelves termed nasal conchae (unseen). The airways inferior and lateral to the conchae are referred to as meatuses. Each meatus is named for the concha that lies above it e.g., superior concha, superior meatus. The meatuses are very narrow. The nasal topology is slightly asymmetric *(Asymmetry between the right and left nasal cavities is a general aspect common at least for all mammals).*

The nasal passages of the chimpanzee consisted of two airways (Fig. 5.1-A) separated by a narrow septum, which was roughly planar. The septum extended through the central nasal passages from the end of the nasal vestibule till the anterior of the nasopharynx. In the nasopharynx/pharynx region, the airways continued straight horizontally without bending (Fig. 5.1-D). The chimpanzee has downward-projecting forward-facing nostrils. Air enters through the circular shaped nostril openings (Fig. 5.1-C), the surfaces of which begin at the forward tip of the nose.

The nasal airways are bounded by the septum on the medial side, the dorsal wall above, the ventral floor below, and the lateral wall on the outside. There were three geometrically distinct regions of the nasal airways: nasal vestibule, central nasal passages, and nasopharynx (Fig. 5.2), each of which exhibits characteristic flow patterns.
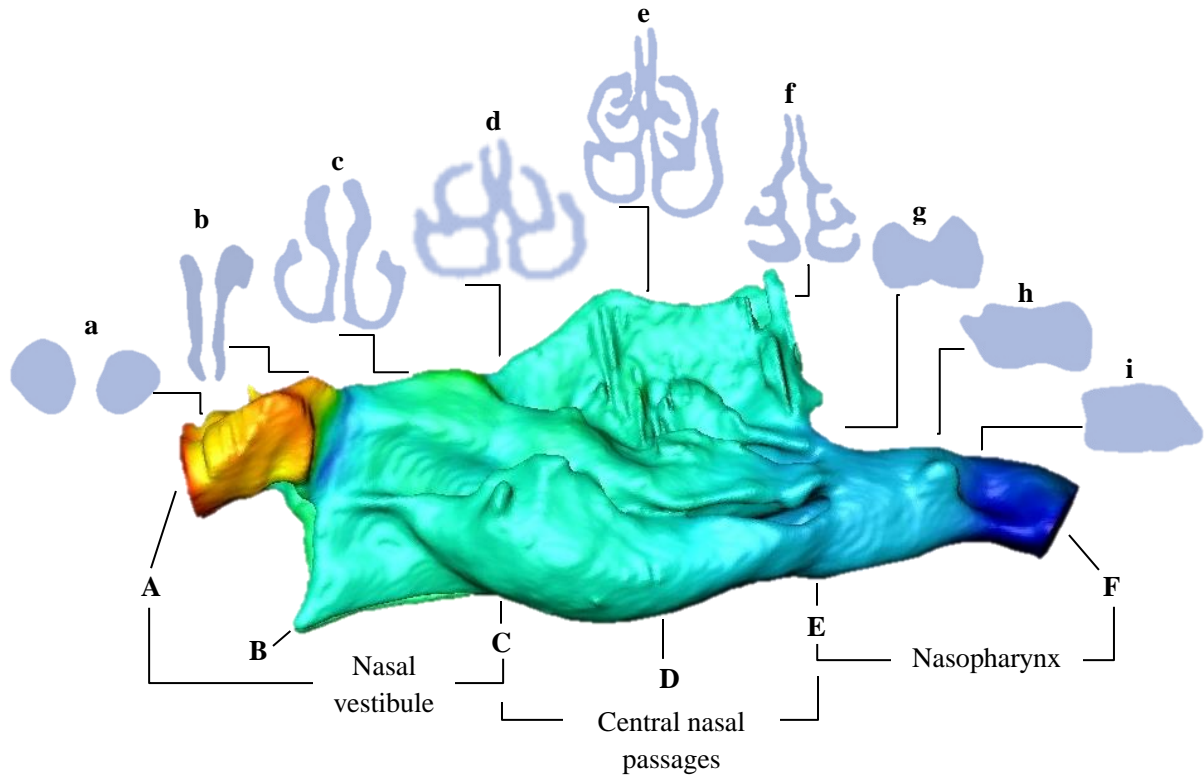
Figure 5.2 Lateral view of the chimpanzee nasal airways. Nine representative sections are also shown in frontal view. Sections are labeled (a-i) and will be referred to in the text. Features of interest include the nostrils surface *(A)*, nasopalatine duct *(B)*, anterior margin of the middle turbinate *(C)*, inferior meatus on the ventral and lateral side of the inferior turbinate *(D)*, posterior extent of the septal wall *(E)*, and outlet *(F)*. Three characteristic airways regions are also indicated as nasal vestibule, central nasal passages, and nasopharynx.

5.1.1 Nasal vestibule

We define the nasal vestibule as the region which extended from the frontier of the nostrils to the beginning of the middle turbinate (Kepler, et al., 1998). Starting at the anterior margin of the nose, airways cross sections were small and roughly circular in shape (Fig. 5.2, section a). Moving posteriorly, the shapes of the cross sections became more elongated (Fig. 5.2, section b). The protrusion of the anterior portion of the inferior turbinate into this airways created curved lateral walls thus the appearance of a curved channel designated the inferior meatus (Fig. 5.2, section c). The inferior turbinate is the largest (House, et al., 1966), spanning nearly the entire length of the

39

main nasal passage. Progressing toward the central nasal passages, cross sections narrowed, elongated, and became more complex (Fig. 5.2, section d). The protrusion of the middle and superior turbinates into the nasal airways created curved lateral walls.

5.1.2 Central nasal passages

The central nasal passages started with the anterior margin of the middle turbinate and extend posteriorly for the full extent of the inferior, middle, and superior turbinates. The middle turbinate was almost as large as the inferior turbinate while the superior turbinate was much smaller, only about half the length of the middle turbinate, and was in the posterior part of the main nasal passages. This region of the airways was characterized by long and narrow cross sections. These channel-like airways (Fig. 5.2, section d) were created by the protrusion of the inferior and middle turbinates into the nasal passages. The turbinates protruded into the nasal passages with the airways curling around them ventrally and laterally in a manner that gave the airways' cross sections a more complex shape (Fig. 5.2, section e). Due to the presence of the turbinates, the cross-sectional perimeter increased (Fig. 5.2, sections d-f). At the posterior end of the main nasal passage, the turbinates and the septum at the same point end and the two cavities merged into one (Fig. 5.2, note E). This region marked the choanae which is the beginning of the nasopharaynx. The cross section area of the airways at this point was inclusive of the two sides of the nose (Fig. 5.2, section g).

5.1.3 Nasopharynx

The portion of the airways designated as nasopharynx contains a small portion of the posterior nasal passages in addition to the true nasopharynx (Kepler, et al., 1998). The central nasal passages ended and the nasopharynx region began at the point where the dorsal wall drop abruptly (Fig. 5.2, note E). The two halves of the nasal cavity joined at the point where the septum ended (Fig. 5.2, section

g). In this region, the cross-sections more roughly resembled sections of an ellipse-shaped tube (Fig. 3, sections g-i).

5.2 Discussion

The nasal passage of chimpanzee is long and triangular as seen from a side view, and its nasal vestibule is horizontal and vertically connected to the middle of the nasal passage (Losken, et al., 1994).

A comparison of the results in the chimpanzee computer model to results from experimental and/or computer models of human and rhesus monkey nasal airways is important because of the anatomical similarities between all three species.

The nasal cavity within the facial cranium of chimpanzee and rhesus monkey was triangular-shaped in the lateral view (Losken, et al., 1994). This pattern contrasts with that found in human, who possessed a quadrangular-shaped nasal cavity (Losken, et al., 1994). Results presented by Losken et al., (1994) in its comparative study of nasal cavity patterns in chimpanzee, rhesus monkey and human showed a longest and highest nasal cavity in chimpanzee. House, et al., (1966) reported that the area between the superior nasal concha and the roof is larger in chimpanzee than in human. Human nasal cavity is longer and taller than that in rhesus monkey (Losken et al., 1994).

Our observation of three distinct regions in the chimpanzee nasal airways corresponds to observations of Schreck, et al., (1993) done on 3x plastic replica of human nasal airways, and Kepler, et al., (1998) done on a right nasal airway computer model of rhesus monkey. In their analysis of flow fields in human and rhesus monkey airways, they also partitioned the airways into three compartments which are equivalent to the nasal vestibule, central nasal passages, and nasopharynx of the chimpanzee.

41

Cross-sectional areas in the nasal vestibule of the chimpanzee and human (Schreck, et al., 1993) nasal airways decreased up to the point of the nasal valve and then increased, whereas cross-sectional areas in the nasal vestibule of the rhesus monkey increased monotonically (Kpeler, et al., 1998; Morgan, et al., 1991).

The nostrils in chimpanzee were horizontal (Nishimura, et al., 2016). However human nostrils were vertically oriented (Kumahata, et al., 2010; Hanida, et al., 1013) and rhesus monkey exhibited expanding nostrils (Morgan, et al., 1991; Kepler, et al., 1998). The horizontal nostrils in chimpanzee were connected vertically with the middle of the nasal cavity (Nishimura, et al., 2016) whereas the human ascending nostrils were connected close to the floor of the nasal cavity (Losken, et al., 1994).

A nasopalatine duct was found in chimpanzee (Smith, et al., 2001; Nishimura, et al., 2016) and rhesus monkey (Morgan, et al., 1991; Kepler, et al., 1998) nasal topologies. This feature wasn't observed in human nasal cavity studies.

In the nasopharynx/pharynx, the airways made a 90° bend toward the larynx in human (Kumahata, et al., 2010; Hanida, et al., 2013) and rhesus monkey (Kepler, et al., 1998). This feature was not seen in chimpanzee where the airways remained horizontal in nasopharynx/pharynx region without bending.

Kepler, et al., (1998) and Morgan, et al., (1991) found that the ventral floor of the nasal vestibule in rhesus monkey made approximately a 45° angle with the ventral floor of the central nasal passages. This feature wasn't reported in human and chimpanzee nasal airways. We attribute this characteristic to the monotonically expanding nasal vestibule found in rhesus monkey.

CHAPTER VI

NASAL AIRFLOW AND AIR-CONDITIONING IN CHIMPANZEE

6.1 Introduction

CFD method was implemented to mimic the airflow pattern and the temperature, humidity, and water distributions inside chimpanzee nasal cavity model derived from CT scans. The technique of CFD is fully developed and commonly applied in fluid studies of human and animals, including the simulation of the body heat, the blood flows in arteries and the airflow in respiratory tract (Oldham et al., 2000; Saber et al., 2003; Moore et al., 2005; Xu et al., 2006). The accuracy and the reliability of the simulation results generated by the CFD method are high. An increasing amount of experiments now rely on the simulation results of CFD to save time and resources required in performing *in vivo* experiments. The application of CT scans and CFD method provides a non-invasive alternative with great flexibility and capability of computational approach in measuring physical quantities inside the nasal cavity and simulating nasal airflow patterns.

6.2 Computational flow model

With the aid of FLUENT (ANSYS Inc., Canonsburg, PA, USA), we simulated a laminar steady airflow state. We investigated the airflow within chimpanzee nasal passages during an inhalation stage. A steady laminar state is logic for a normal breathing frequency corresponding to a flow rate at resting phase. Turbulence doesn't interfere in the current study because critical Reynolds number cannot be reached by the airflow inside the nasal cavity as we are treating a rest breathing case. Assumption of incompressible flow is allowed at normal physiological flow rates (Vogel, 1994). The physiological model used here is based on incompressible, viscid, laminar air flow model considering heat and water transfer, developed by Kumahata, et al. (2010) (Kumahata, et al., 2010). We adapted it to reflect chimpanzee respiratory physiology.

The governing equations include the equation of momentum conservation (1), the equation of mass conservation (2), the energy transport equation (3), and the water mass fraction transport equation (4).

$$\rho\{\partial u/\partial t + (u \cdot \nabla)u\} = -\nabla p + \mu\nabla^2 u \tag{1}$$

$$\nabla \cdot u = 0 \tag{2}$$

$$\rho C_p\{\partial T/\partial t + (u \cdot \nabla) T\} = K\nabla^2 T \tag{3}$$

$$\partial F/\partial t + (u \cdot \nabla)F = D\nabla^2 F \tag{4}$$

where ρ, u, t, p, μ, C_p, T, K, D, and F indicate density, velocity, time, pressure, dynamic viscosity, specific heat, temperature, thermal conductivity, coefficient of mass diffusion, and mass fraction of water, respectively. We resolved the above system of equations with the aid of the software FLUENT (ANSYS Inc., Canonsburg, PA, USA) using the finite volume scheme.

6.3 Boundary conditions

Nares were considered free inlets. Thermal conductivity was set to 0.0454 W/mK and the coefficient of mass diffusion of the inspiratory air was set to 2.88 x 10^{-5} m^2/s. The nasopharynx velocity boundary equals the outward flow velocity. During an inspiratory phase under a steady state, the time-averaged velocity was set to 1.4 m/s. This value was determined with a nasopharyngeal cross-section's area of 1.62 cm^2, a breathing rate of 18 respiratory/min (Worthington, et al., 1991) and a tidal volume per breath equals 294.6 ml (Stahl, 1967). Nasal lining was considered rigid where no-slip boundary condition was set for the fluid velocity.

The nasal tissue layer's temperature T_o was set to the body temperature, 34 ℃. At a relative humidity of 100%, nasal tissue layer's water mass fraction F_o equaled 3.34%. Nasal epithelial layer's thermal conductivity K_{memb} was 0.6 W/mK (Lervik, et al., 2010). The coefficient of mass diffusion of the epithelial layer, as a high density-water vapor source (Lee, et al., 1954), D_{memb} equaled 2.6 x 10-5 m^2/s. Figure 6.1 illustrates the material properties and the boundary conditions.
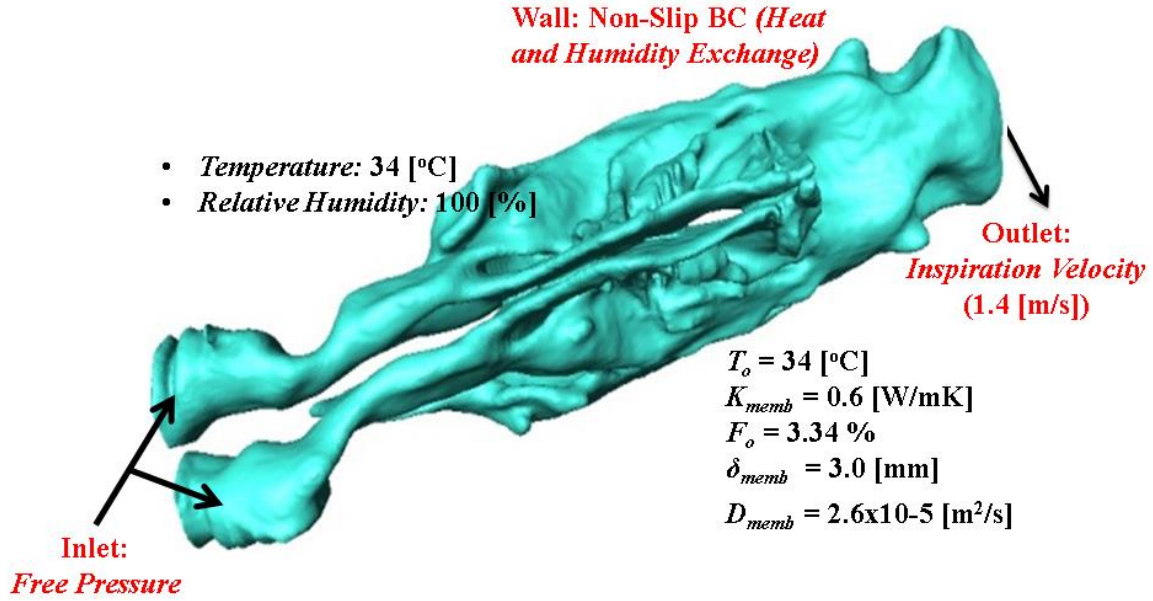
Fig. 6.1 Boundary conditions for numerical simulation: Nasopharynx/pharynx was assigned an outward velocity of 1.4 m/s. Nares were treated as free inlets. Nasal cavity lining had a non-slip boundary. T_o, K_{memb}, F_o, δ_{memb}, D_{memb} indicate the tissue layer's temperature, thermal conductivity of the epithelial layer, tissue layer's mass fraction of water (under relative humidity of 100% at 34°C), epithelial layer's thickness, and mass diffusion coefficient of the epithelial layer, respectively.

At nasopharyngeal level, time-averaged velocity of the inspiratory airflow was determined using the nasopharynx/pharynx cross-section's area, the breathing rate (Worthington, et al., 1991), and the tidal volume at rest state (Stahl, 1967) (see Table 6.1). The area of nasopharynx/pharynx cross-section was determined from CT scanning with the aid if the software Magics.

Tidal volume at rest state was calculated referring to the following equation (Stahl, 1967).

$$TV = 7.69BW^{1.04} \tag{5}$$

where *TV* and *BW* denote the chimpanzee tidal volume at rest and its body weight, respectively.

The breathing rate was calculated referring to the following equation (Worthington, et al., 1991).

$$f = 0.84BW^{-0.28} \tag{6}$$

46

where *f* and *BW* denote the chimpanzee breathing rate at rest and its body weight, respectively.

Time-averaged velocity was determined using Eq.7.

$$FV = (2f \times TV)/CA \tag{7}$$

where *FV, f, TV* and *CA* denote time-averaged velocity of the nasal flow, breathing rate, tidal volume, and cross-section's area at the nasopharyngeal/pharyngeal region of the chimpanzee, respectively.

Table 6.1 Subject, scans, and estimated parameters of respiration

Studied subject	Specie's name	Pan troglodytes
	Common name	(Common) Chimpanzee
	Gender	Female
	Estimated age	35 year-old (Adult)
	Body Weight	44.1 Kg
Scans	Modality	CT
	Number of scans	401 slices
	DICOM format	512 x 512 pixels
	Resolution	0.351 mm/pixel
	Pitch between scans	0.5 mm
Respiratory parameters	*CA*	162 mm^2
	TV	394.6 ml
	f	0.3 Hz
	FV	1.41 m/s

Abbreviations. CT: Computed Tomography, CA: Cross-section's Area at nasopharyngeal/pharyngeal boundary, TV: Tidal Volume, f: breathing rate, FV: nasal air Flow Velocity at nasopharyngeal boundary.

6.4 Computational parameters

Simulation of steady state airflow inside the chimpanzee nasal airways during an inhalation phase was performed with the aid of FLUENT (ANSYS Inc., Canonsburg, PA, USA). Numerical computation was performed with implicit time stepping and a pressure based solver. Pressure-velocity coupling was accomplished with SIMPLE approach. Green-Gauss Cell Based gradient option was employed to determine spatial gradient. Second Order and Quick discretization schemes were employed for pressure and other remaining variables respectively. Computation was run on an Appro PC Cluster (24 core Large Memory Node Appro 1143H) consisting of AMD Opteron 2.6 GHz CPU running the Redhat Linux operating system with 128 GB memory. Parallel computation was performed using the parallelization tool of FLUENT. Convergence was obtained after less than 250 iterations done on 6 processors, requiring a total time of around 2.5 hours. A norm inferior to 10^{-6} was set as convergence criterion to terminate the iterations of energy; other norms were inferior to 10^{-5} except for the water mass fraction which was set to less than 10^{-3}. The under relaxation factors were kept as default. Graphical results were displayed using Avizo 7.0.

6.5 Flow patterns

CFD simulation was performed using standard ambient atmospheric conditions i.e., the temperature of inhaled air was 25 ºC at a relative humidity of 35%.
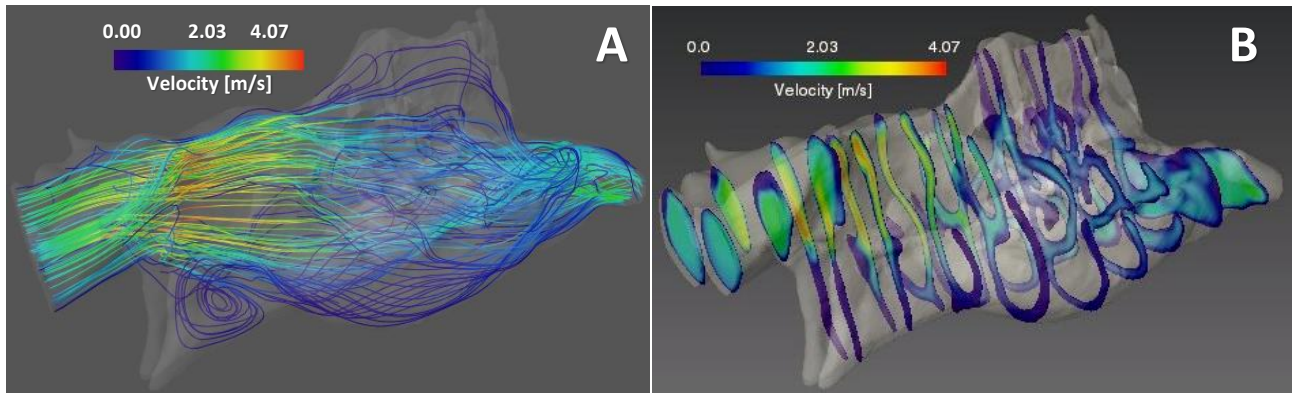
Figure 6.2 Inspiratory flow structure and flow velocity of chimpanzee nasal passages: The streamlines (A) and the contours planes (B) indicate the air streams direction and velocity distribution within the nasal airways, respectively. The middle meatus passed the largest flow rate. The inferior meatus passed lesser flow rate. Smallest airflow rate was observed in the superior airways. Highest velocity was seen around the nasal valve region.

The streamlines in Fig. 6.2-A demonstrate the spatial pattern and direction of the air flow filed. The scalar quantity representing the velocity magnitude was illustrated using contours (Fig. 6.2-B). The different colors in both illustrations reflect the range of airflow velocity magnitude thru the chimpanzee nasal airways.

Generally, the flow can be defined either by its location into the intricate geometry or by its classification such as vortices and/or streamlined. The protrusion of the inferior, middle, and superior turbinates into the central nasal airways produce distinguishable meatuses. Moreover, the cross sections of the nasal vestibule and the nasopharynx regions are relatively simple. Thus the streamlined flow inside the nasal cavity would be better designated by the meatus over which it flows (*e.g.*, superior or inferior lateral).

A highest velocity flow was noticed around the nasal valve area. Middle meatus, sandwiched between the inferior turbinate and the middle turbinate passed the largest flow rate with high velocity. Inferior meatus, located below the inferior turbinate passed lesser flow rate than the middle meatus. Superior meatus, stuck between the middle turbinate and superior turbinate passes the least flow rate at lowest velocity. The reason behind the latter fact is the protection of the

olfactory region which is sited in the upper airways of the nasal passage. The current work simulated a rest-breathing state; in case of sniffing state, predicted simulation of the flow in the upper airways should be quite different.

6.5.1 Nasal vestibule

Flow throughout the nasal vestibule region was horizontally straight except of the swirl appearing in the nasopalatine region. Most of the air entering the front middle region of the nostrils flowed, without deviating, alongside the septal lining to the mid-medial, mid-lateral, and, slightly lesser, superior margin of the central nasal airways. Dorsal airstreams appeared as detachment from the air entering the lateral portion of the nostrils. Flow in the superior airways was slower than the middle streams. Streams coming from air that entered to the inferior lateral portion of the nostrils formed the ventral anterior vortex as the streams impinged upon the nasopalatine duct region's wall. While leaving the nasopalatine duct region at low velocity, the swirling flow diverged toward the ventral and lateral paths of the inferior meatus.

6.5.2 Central nasal airways

The flow in the mid region of the nasal passage looked streamlined and slowed down after leaving the nasal vestibule. The dorsal vortex is a subset from the superior lateral portion of nostrils' streams. In general, streams entering from the dorsal, middle, and inferior margins of nostrils' surface flowed toward the dorsal, middle, and inferior meatuses, respectively. However, lateral and medial streams did not forcibly flow toward medial and lateral portions of the meatuses. The amount of flow differed amongst the meatuses of the central nasal airways. The middle meatus (middle medial and middle lateral) had the largest volumetric flow. The dorsal flow represents the smallest fraction of the overall flow.

6.5.3 Nasopharynx

The disappearance of the superior meatus, as the dorsal wall drop abruptly and the septum ended, caused a bulky ventral flow bordered by central nasal airways and nasopharynx. The flow throughout the nasopharynx region kept horizontally streamlined without bending.

6.6 Air-conditioning distributions
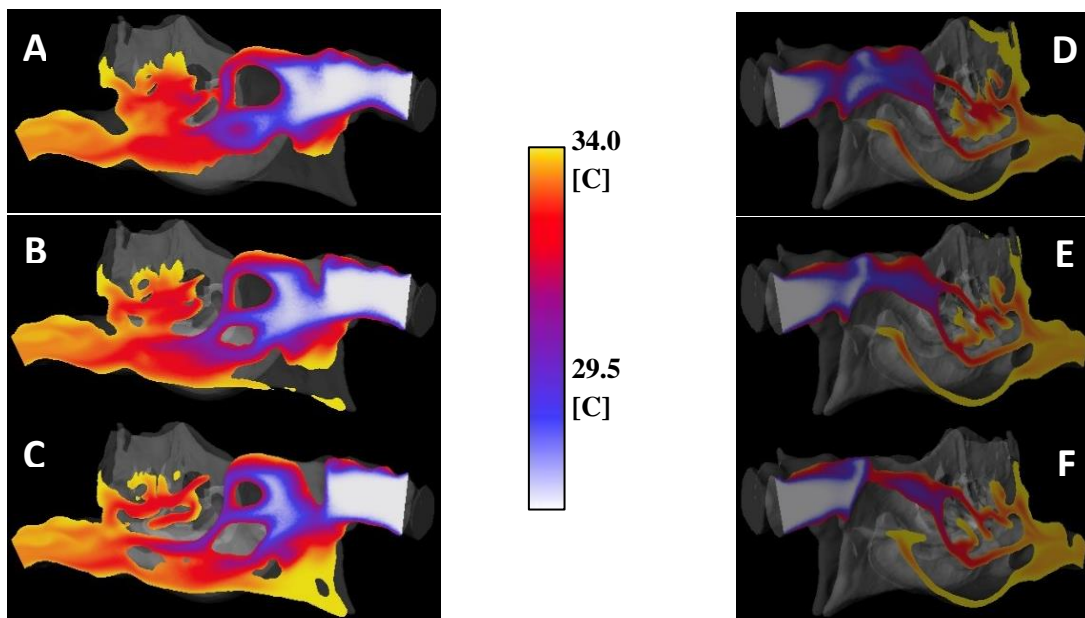
Figure 6.3 3D views of the temperature distribution inside the nasal passage (inhaled air: Temperature = 25 °C, relative humidity = 35%). The left panel (A-B-C) of contour plans are sagittal sections of the right nasal passage outbounding from the middle of the right nasal airways (top) to outward (down). The right panel (D-E-F) of contour plans are sagittal sections of the left nasal passage outbounding from the septal side (top) to the middle of the left nasal airways (down). There is no relation between the locations of the sagittal sections in the right and left panels. The airflow temperature is higher near the nasal lining.

Figure 6.3 shows 3D views of temperature distribution within the chimpanzee right nasal passage (left panel) and left nasal passage (right panel) in different sagittal plans outbounding from septal side (top) to outward (down). The temperature increases slowly within the nasal vestibule region, but increases gradually through the central nasal passages. The inspiratory air was warmed plenty

to near body temperature (34 ℃) by reaching the posterior margin of the nasopharynx region. Furthermore, the tendency observed for warming the inhaled air in various sagittal plans is different. The rate of warming the inhaled air decreases while approaching the sagittal medial portion of the right nasal passage (Fig. 6.3 C-A) and the sagittal medial portion of the left nasal passage (Fig. 6.3 D-F). Indeed, the temperature of inspiratory air was attuned by heat transfer through nasal epithelial layer. This explains the fact that inhaled air temperature increases faster near the nasal cavity lining. The high tissue-side temperature (34 ℃) allows a quick heat exchange with the airflow close to nasal airways lining. The higher tissue-side temperature (34 ℃) allows a quick heat exchange with the airflow.
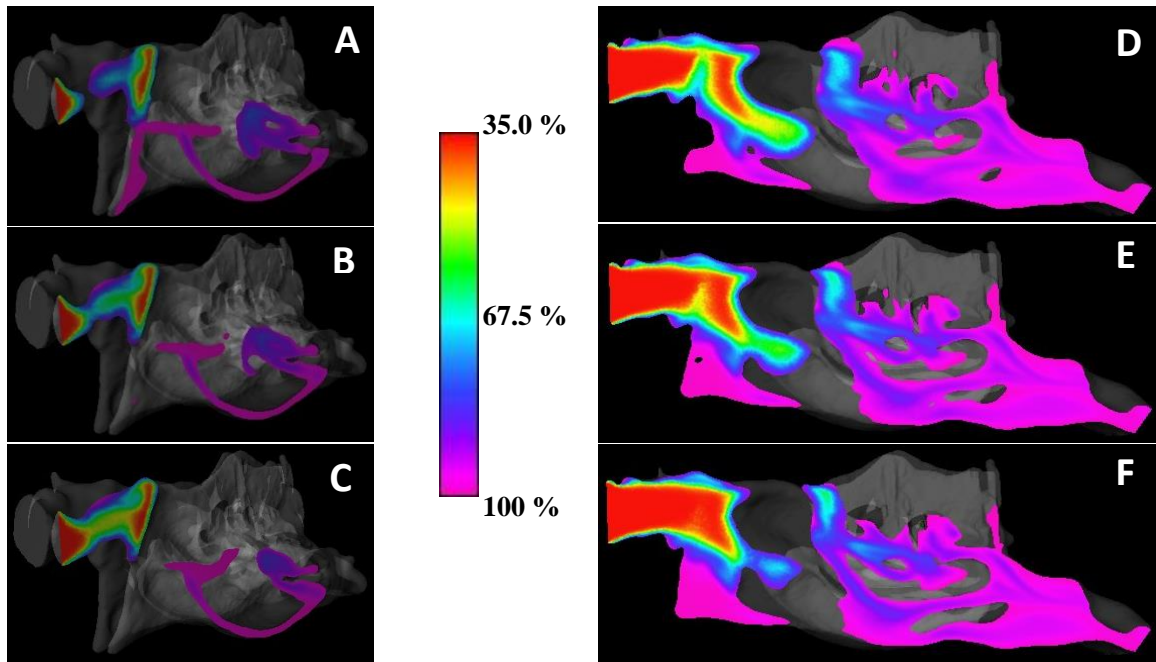
Figure 6.4 Relative humidity distribution inside the nasal passages (inhaled air: Temperature = 25 ℃, relative humidity = 35%). The contour plans are cross sections of the right nasal cavity (right panel, 2D views) outbounding from outward (top) to the middle of the right nasal airway (down), and left nasal cavity (left panel, 3D views) outbounding from septal side (top) to the middle of the left nasal airway (down). There is no relation between the locations of the sagittal sections in the right and left panels. The airflow relative humidity is higher near the nasal cavity lining.

Figure 6.4 shows a 3D view of the relative humidity distribution inside the chimpanzee left nasal cavity (left panel) at different sagittal plans outbounding from the septal side (top) to the medial of the left nasal airway (down), and 2D view of the relative humidity distribution inside the chimpanzee right nasal cavity (right panel) at different sagittal plans outbounding from the outward (top) to the medial region of the right nasal airway (down). The relative humidity increased slowly within the nasal vestibule region. Through the central nasal passages, relative humidity augmented gradually and inspiratory air got adequately moistened to roughly 100% before reaching the posterior margin of nasopharynx region. In addition, the tendency of humidifying the inhaled air observed in the various sagittal plans is different. The rate of humidifying the inhaled air decreased while approaching the sagittal medial plans of the right and left nasal cavities. Indeed, moistness of inspiratory air got attuned as a result of water transfer through the nasal epithelial layer. Hence inhaled air's relative humidity increased faster near the nasal lining. High tissue-side relative humidity (100 %) allowed a quick exchange of water with the airflow.

6.7 Discussion

Chimp's nasal cavity is divided into an upper olfactory region (Jankowski, 2012) and lower respiratory region (Figure 6.2).

The highest velocity of nasal airflow was in nasal valve region. Moving posteriorly, the airflow velocity slowed down. Indeed, the protrusion of the turbinates in the central nasal airways streamlined the flow into narrow channels (meatuses). The meatuses cross-sections perimeters increased in the central nasal airways. Thus flow's average velocity is less than that in the nasal valve region.

The present CFD model showed that in chimpanzee nasal cavity the air flows horizontally and straight forward from the vestibule, over the central nasal passages, and out through the

nasopharynx (see Fig. 6.2) without bending at the pharynx region. In addition, the air passes through the middle medial and middle lateral trajectories in greater volume and at faster velocity compared with the inferior and upper paths of the nasal airways (see Fig. 6.2A-6.2B). The inferior meatus, i.e. the path beneath the inferior nasal turbinate, passed lesser airflow rate. Superior airways where the olfactory region is located passes the smallest amount of air at low velocity. Our model showed a diffusive fast airflow over the nasal valve, and a relatively large and a minor vortices of air swirling, at low velocity, inside the nasopalatine duct region and the anterior dorsal airways, respectively.

6.7.1 Comparison of nasal airflow to human and rhesus monkey

The present CFD simulation showed that in chimpanzee the streamlined inhaled air flowed straight forward from the vestibule, over the nasal passage, and out to oropharynx. The main airflow path within chimpanzee nasal cavity was in the mid-medial and mid-lateral paths of the central nasal passages. Airflow patterns in the nasal airways of chimpanzee differed from that in human and rhesus monkey. A recent study (Zhu, et al., 2011) in nasal cavity airflow of different humans exhibiting various external noses and nostrils showed that the inhaled air in human flowed "upward along the ascending vestibular region into the nasal cavity and downward to the oropharynx". The same study reported that the air flowed over the middle medial to inferior portion at larger volume and faster velocity comparing to peripheral and superior paths in human nasal airways. Previous experimental (Morgan, et al., 1991) and computer simulation (Kepler, et al., 1998) studies done to rhesus monkey determined secondary flows anterior to the nasal passage and streamlined flow posteriorly, major flow passage was observed in the ventral (mid-medial and mid-lateral) paths of the central nasal airways. Secondary flow noticed in nasal vestibule of rhesus monkey was attributed to the monotonically expansion of airway cross-sections in the nasal vestibule (Kepler, et al., 1998).

Our simulation showed the highest average speed in the nasal valve area, similar to numerical results done on human nasal cavity (Kumahata, et al., 2010; Hanida, et al., 2013).

As in chimpanzee, a ventral anterior vortex was seen in rhesus monkey (Morgan, et a., 1991) but not in human. The absence of the anterior ventral vortex in human nasal passages may be attributed to the absence of the nasopalatine duct in human nasal topology.

The expansion of nasal cavity anterior to the central airways region is common to all three species. Schreck and coworkers (Schreck, et al., 1993) attributed the formation of vortex in their human model to this expansion of the airway. They noticed a vortex near the olfactory region of their model, which diverted a stream at high velocity from olfactory membrane. Zhao, et al., (2004) reported the existence of vortices in the upper meatus within the human nasal passage. Kepler, et al., (1998) and Morgan, et al., (1991) observed a dorsal anterior vortex in rhesus monkey. Kepler and coworkers (Kepler, et al., 1998) attributed its appearance to the expansion of airway cross-section in the nasal vestibule region. It is similar to the dorsal vortex observed in our chimpanzee nasal airways model. Alike to Schreck, et al., (1993) and Kepler, et al., (1998), the anterior dorsal vortex in chimpanzee appeared to divert great velocity airstream from olfactory membrane. We do also believe that the expansion of the airways at the frontal portion of central nasal passages caused the formation of the dorsal vortex. For all three species, low air velocity was found in the olfactory region.

6.7.2 Analysis of the air-conditioning efficiency
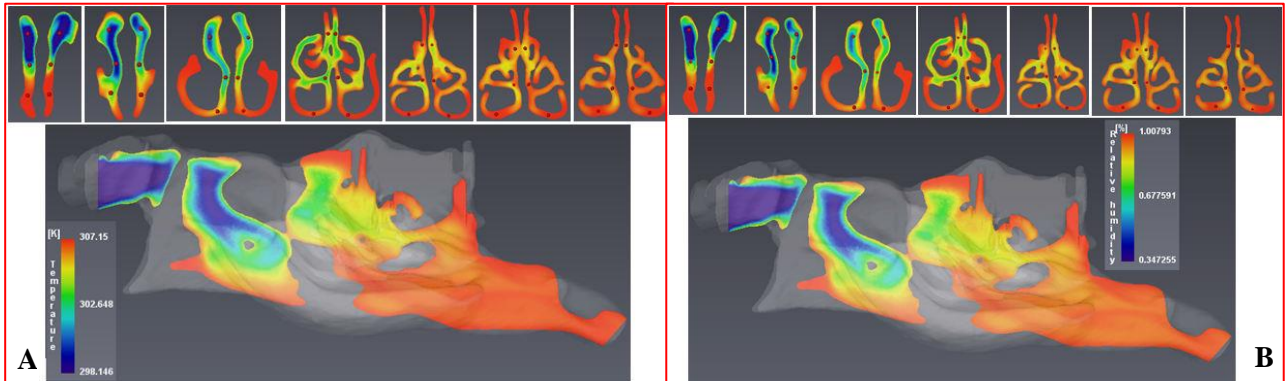
Figure 6.5 (A) Temperature distribution inside chimpanzee nasal cavity: Initial temperature of the inspiratory air was less than the body temperature. The inhaled air got gradually warmer while approaching the nasopharyngeal region by absorbing heat from nasal tissue layer via the nasal epithelial layer. By reaching the nasopharynx, the air, initially inspired at 25 ℃, was heated to approximately the nasal tissue layer's temperature, 34 ℃. (B) Relative humidity distribution inside chimpanzee nasal cavity: Initially inhaled air had a relative humidity equals 35%, whereas humidity in the nasal passage lining is 100%. The air got moistened by absorbing water from the nasal tissue layer via the nasal epithelial layer. The inhaled air got gradually humidified while approaching the nasopharyngeal region. By reaching the nasopharynx, the dry inspiratory air was moistened to almost the nasal tissue layer's relative humidity, 100%.

Similar points relative to the right and left nasal cavities were chosen for temperature and relative humidity measurements. Results showed similarities in temperature and humidity patterns in the three airways (lower, middle, upper) between right and left nasal passages, respectively.

Graphs of temperature and humidity distributions are for one representative nasal passage (left nasal cavity), because both cavities showed comparable air-conditioning structures.

The following graphs show temperature distribution and humidity distribution of the left nasal passage in lower, middle, and upper airways, respectively. In both graphs, the horizontal axe represents the distance from nostrils tip [in cm]. The vertical axes represent the temperature [in ºK] and the relative humidity [%], respectively. In Fig. 6.5-A and Fig. 6.5-B, red dots appearing in the coronal sections indicate the measurement points where temperature and relative humidity were

respectively determined. Asymmetry between the right and left nasal cavities is a general aspect common at least for all mammals. Humidity and temperature have similar patterns through the nasal cavity.
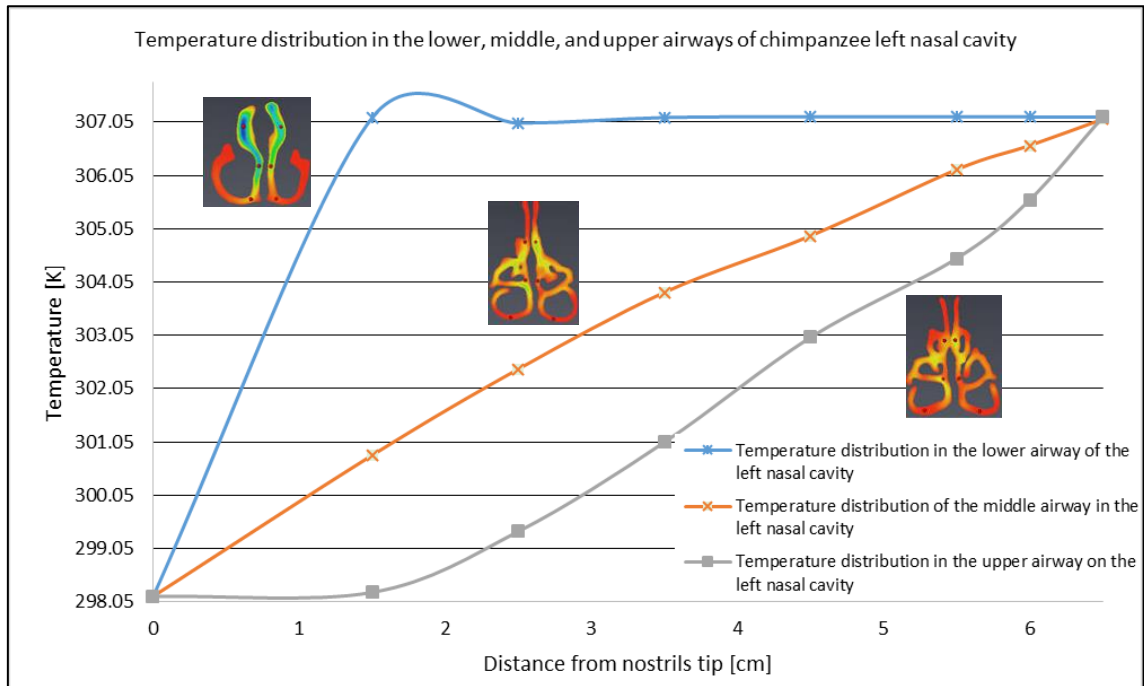
Figure 6.6 Temperature distributions inside chimpanzee nasal cavity: Temperature distribution in the lower airway of the left nasal cavity (blue dots); Temperature distribution in the middle airway of the left nasal cavity (orange crosses), and temperature distribution in the upper airway of the left nasal cavity (grey squares).
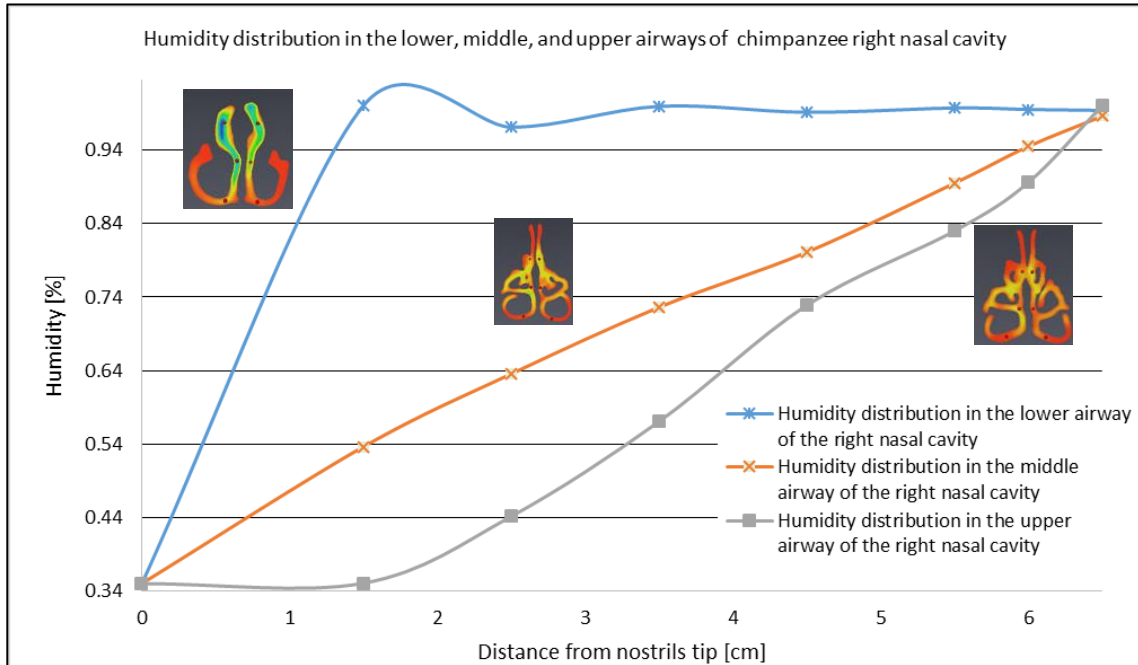
Figure 6.7 Humidity distributions inside chimpanzee nasal cavity: Humidity distribution in the lower airway of the left nasal cavity (blue dots); Humidity distribution in the middle airway of the left nasal cavity (orange crosses), and humidity distribution in the upper airway of the left nasal cavity (grey squares).

Here, we do only report the data related to the left nasal cavity which appeared more readable. Temperature and humidity adjustments of inspiratory air behave differently in each transversal site of the nasal airways.

Temperature's and humidity's patterns of the lower airway may be approached by a rotational curve; i.e. the inhaled cooler and dryer air within lower airway of the nasal passage tended to get warmed and moistened at once within short distance from the inlet. The respective curves showed that after reaching quickly a maximum, the temperature and humidity decreased slightly and then maintained to the body temperature and humidity values while increasing distance from the nares. The reason behind such structure of inhaled air conditioning is the protrusion of the anterior portion of the inferior turbinate into this airway which created curved lateral walls thus enhancing air-

conditioning when surrounded by mucosal nasal lining. The inferior turbinate is the largest (House, et al., 1966), spanning nearly the entire length of the main nasal passage.

Temperature and humidity patterns in the middle airway followed a logarithmic curve (Nishimura, et al., 2016), the constant conditioning of the inhaled air was sustained by the consecutive turbinates' protrusion inside the nasal cavity (Inferior, middle, and superior turbinates respectively).

Unlike the lower airway, in the upper airway the inhaled air kept the same initial temperature and humidity for a while before starting to get warmer and moistened following a linear curve. This air-conditioning delay is due to the fact that the superior turbinate, main feature to condition the inhaled air in the upper airways appears only in the latter portion of the main nasal passage and is only about half the length of the middle turbinate.

Reaching same level close to nasopharynx, the temperature and humidity distributions have the maximum values in the lower airway and the lowermost values in the upper airway. However, both right and left nasal cavities merge together into a narrow region of the nasopharyngeal cavity, where the three transversal distributions should be mixed together.

6.8 Model's accuracy and reliability

Our developed computer model is accurate because of the small pitch between scans and the CFD model is reliable due to the use of higher order discretization schemes, accurate convergence criteria ($<10^{-6}$) and the increased resolution of the mesh.

The model used by Nishimura, et al. (2016) aped a 0.5 mm thickness of nasal epithelial layer, which was in reality specific to simulate the air-conditioning performance within human nasal cavity (Hanida, et al., 2013). Thus their simulation results may not imitate accurately the nasal air-conditioning of small-bodied chimpanzee, having thinner nasal epithelial layer that allows more efficient air-conditioning compared to the thick nasal epithelial layer of human.

HUMAN vs. CHIMPANZEE: NASAL AIR CONDITIONING

7.1 Numerical experiment

Temperature and relative humidity of inspiratory air got attuned while transferring the heat and water between tissue side and air side thru nasal epithelial layer that covers the nasal cavity lining. We investigated hot-wet (T = 50 ºC, RH = 100%) case, and cold-dry (T = -10 ºC, RH = 10%) case in term of temperature (T) and relative humidity (RH) inspiratory air. Results found in the chimpanzee nasal anatomy were compared to CFD simulations done by Kumahata, et al., (2010) in a realistic reconstructed human nasal topology (Kumahata, et al., 2010). Red dots (Figure 7.1) represent the evaluation points where values of simulated temperature and humidity were determined from chimpanzee nasal cavity.
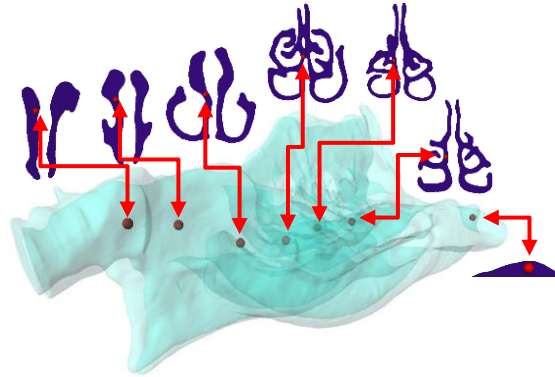
Figure 7.1 Evaluation points of simulation: Kumahata, et al. (2010) determined the temperature and relative humidity in a human computer nasal model; the values were taken at distances of 1.5, 2.5, 3.5, 5.5, and 6.5 cm from the nares. Same parameters were determined at equivalent points (axial direction) of the chimpanzee nasal anatomy.

7.2 Results

For the hot-wet case (case A), temperature was set to 50 °C, relative humidity was set to 100%, and water mass fraction was set to 7.95%. For the cold-dry case (case B), temperature was set to -10 °C, relative humidity was set to 10%, and water mass fraction was set to 0.0175%. Other parameters were kept the same as previous chapter.
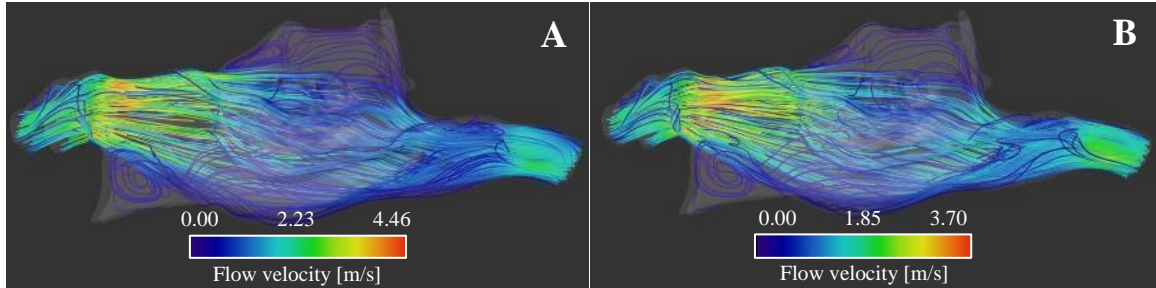
Figure 7.2 Flow inside the chimpanzee nasal cavity of hot-humid (A) and cold-dry (B) inspiratory air: Most air flowed in middle meatus, a lesser rate of air flowed in the inferior meatus. The least airflow was seen over the superior meatus.

Figure 7.2 uses streamlines to illustrate the airflow inside the nasal airways. Same features as in the standard condition inhaled air (Figure 6.2) case, anterior ventral and dorsal vortices have been seen in both hot-humid and cold-dry examples. The maximum airflow rate passed through the middle meatus (middle medial and middle lateral) at with high velocity. A lower airflow rate passed through the inferior meatus at lower velocity. The least airflow rate passed through the superior meatus at lowest velocity. Airflow velocity through the nasal valve, region located immediately next to nostrils, was higher in the hot-wet (Figure 7.2-A) inhaled air compared to the cold-dry case (Figure 7.2-B). The difference in airflow velocities through the nasal valve reflects the variance of total energy aroused because the dissimilarity of inspiratory air temperatures in hot-humid example and cold-dry example. Cold-dry inhaled air (T = -10 ℃, RH = 10%) needs more conditioning inside the nasal cavity than does the hot-wet inhaled air (T = 50 ℃, RH = 100%), thus its velocity through the nasal passages (including the nasal valve region) should be lower to permit enough time for the temperature and humidity to get adjusted properly before reaching the nasopharynx/pharynx region. The above results have been also observed in same simulations done on human nasal airways (Kumahata, et al., 2010).

Figure 7.3 3D view of temperature distribution inside chimpanzee nasal cavity: Hot-wet case (A), cold-dry case (B). Contour planes are coronal cross-sections of the entire nasal airways. The inhaled air was conditioned throughout the nasal lining, and almost adjusted to body temperature by reaching the nasopharynx region.

Figure 7.3 represents 3D views of temperature distribution inside the nasal anatomy using contour planes as axial cross-sections over the entire nasal airways. For the hot-wet example, inspiratory air got cooled while supplying heat to nasal tissue layer via nasal epithelial layer throughout the nasal lining (Figure 7.3-A). In the middle zone of the central nasal airways, inhaled air's temperature decreased gradually while approaching the frontal side of nasopharynx zone. The inhaled air was effectively conditioned in the mid nasal airways. By reaching the nasopharyngeal region, inspiratory air got almost conditioned to body's temperature. It is also noticed that the air temperature was quickly adjusted to the body temperature in the passages near the nasal lining such as ventral, inferior lateral, and dorsal airways. In cold-dry example, inspiratory air got warmed while absorbing heat from nasal tissue layer via nasal epithelial layer throughout the nasal lining (Figure 7.3-B). In the middle zone of central nasal airways, inhaled air's temperature increased gradually while approaching the frontal side of nasopharynx zone. Inhaled air was effectively conditioned in the mid nasal airways. By reaching nasopharyngeal region, Inspiratory air got almost conditioned to body's temperature. It is also noticed that the air temperature was quickly adjusted to the body temperature in the passages near the nasal lining such as ventral, inferior lateral, and dorsal airways.
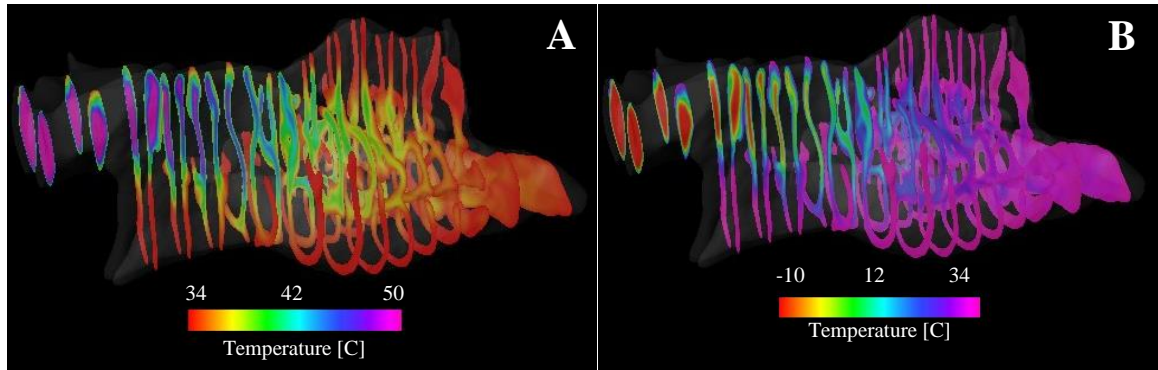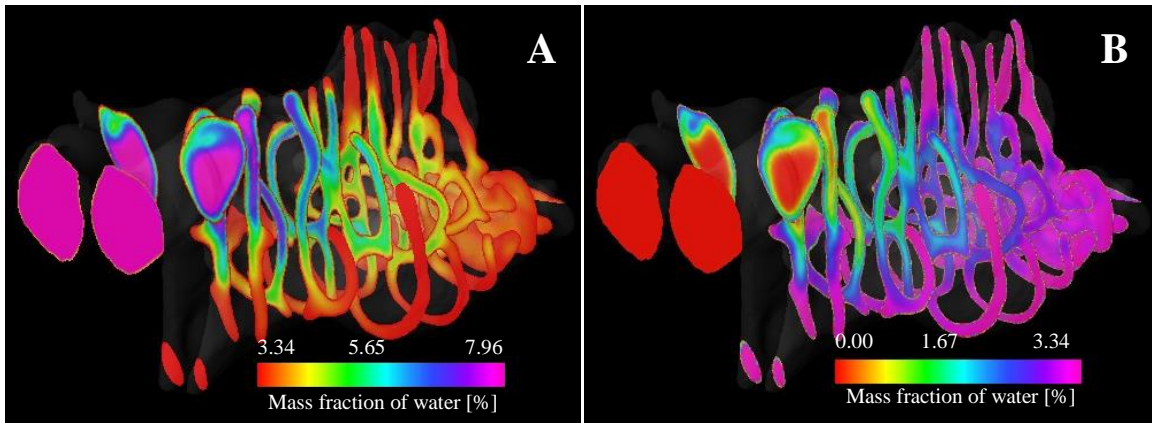
Figure 7.4 3D view of water mass fraction distribution inside chimpanzee nasal cavity: Hot-wet case (A), cold-dry case (B). Contour planes are coronal cross-sections of the entire nasal airways. The inhaled air was conditioned throughout the nasal lining, and almost adjusted to body mass fraction of water by reaching the nasopharynx region.

Figure 7.4 represents 3D views of water mass fraction distribution inside the nasal anatomy using contour planes of axial cross-sections over the entire nasal airways. In hot-wet case, the inhaled air became dry as it delivered water to the nasal tissue layer via the nasal epithelial layer throughout the nasal lining (Figure 7.4-A). In the middle zone of the nasal passages, water mass fraction of the inspiratory air decreased gradually while approaching the frontal region of the nasopharynx. The inhaled air was effectively conditioned in the mid of nasal airways. By reaching the nasopharyngeal zone, inspiratory air was almost conditioned to the body's water mass fraction. We noticed that water mass fraction of inspiratory air was quickly conditioned to body's water mass fraction over passages near the nasal lining such as ventral, inferior lateral, and dorsal airways. In cold-dry example, inspiratory air got moisturized while absorbing water from the nasal tissue layer via the nasal epithelial layer throughout the nasal lining (Figure 7.4-B). In the central region of the main nasal airways, water mass fraction of the inhaled air increased gradually while approaching the frontal side of the nasopharynx zone. The inhaled air was effectively conditioned in the central nasal passages. By reaching the nasopharyngeal region, inspiratory air got almost conditioned to body's water mass fraction of water. It is noticeable that water mass fraction of inspiratory air got

quickly adjusted to the body's water mass fraction within passages near the nasal lining such as ventral, inferior lateral, and dorsal airways.

7.3 Discussion

We reported above simulation results of airflow and heat transfer within the chimpanzee nasal passage using a CFD model developed by Kumahata, et al., (2010) in order to compare nasal air-conditioning effectiveness in human and chimpanzee.

Following graphs show temperature and water mass fraction distributions for hot-wet case and cold-dry case inside human and chimpanzee nasal cavities. In both graphs the horizontal axe represents the distance from the tip of nostrils for both species. The vertical axes represent the temperature (Figure 7.5) and water mass fraction (Figure 7.6) inside human and chimpanzee nasal cavities, respectively.
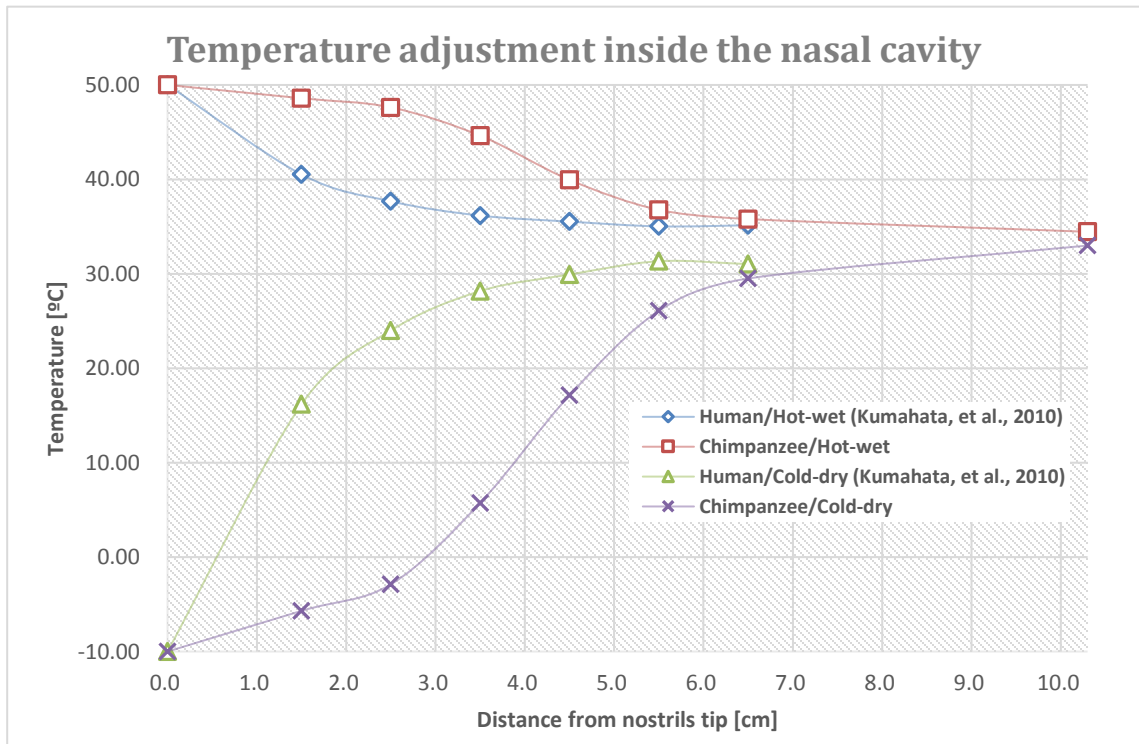
Figure 7.5 Temperature distributions within the nasal cavity: Human/Hot-wet case (blue diamonds), Chimpanzee/Hot-wet case (red squares), Human/Cold-dry case (green triangles), and Chimpanzee/Cold-dry case (purple crosses).

65
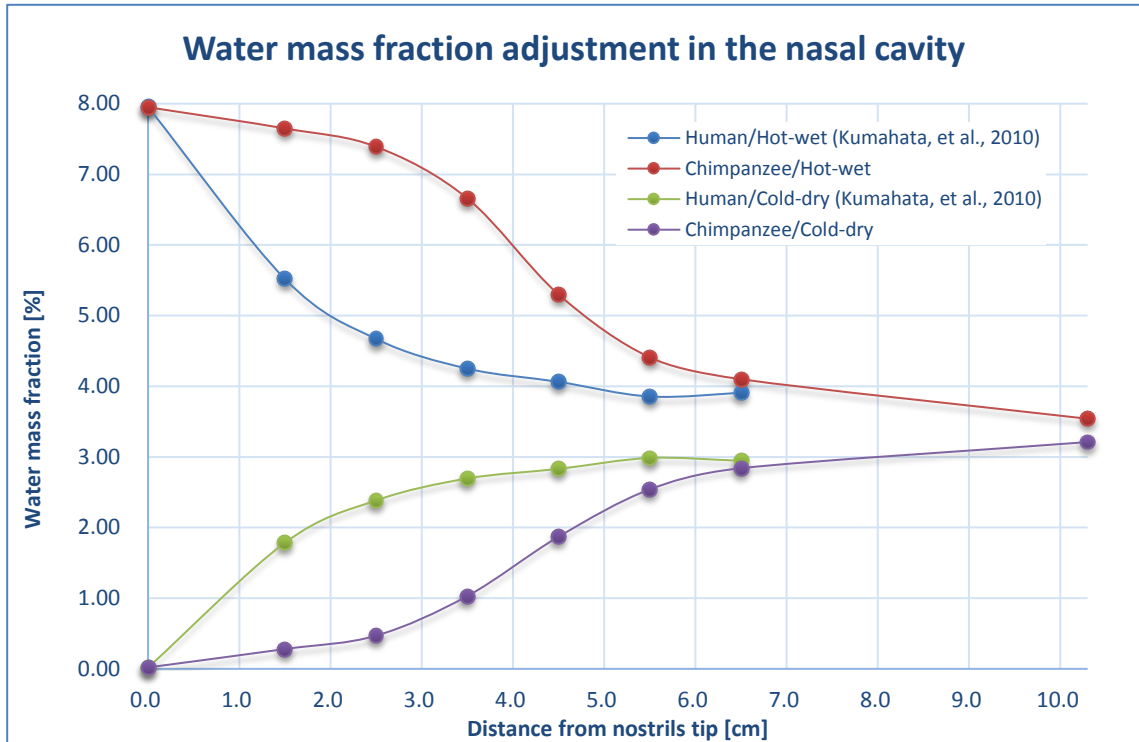
Figure 7.6 Distributions of water mass fraction within the nasal cavity: Human/Hot-wet case (blue dots), Chimpanzee/Hot-wet case (red dots), Human/Cold-dry case (green dots), and Chimpanzee/Cold-dry case (purple dots).

The chimpanzee possesses an elongated face which protrudes afield from the brainpan. The nasal geometry inside the cranium of chimpanzee appeared long and triangular-shaped while seen from side view, and the relatively long horizontal nasal vestibule was attached vertically to the middle of the nasal passage (Losken, et al., 1994). This configuration diverges with human pattern, whose nasal geometry looked quadrangular (Losken, et al., 1994). Losken et al., (1994) reported that the chimpanzee nasal passage was higher and longer than human nasal passage. Results presented by House, et al., (1966) demonstrated that the distance separating the roof from the superior turbinate is bigger in chimpanzee comparing to human.

For both species, inhaled air-conditioning occurred as to decrease/increase the temperature and water mass fraction to around body temperature and water mass fraction by reaching the

nasopharynx region. For human nasal cavity, most air-conditioning occurred in the anterior part of the nasal passage (Kumahata, et al., 2010; Hanida, et al., 2013).

However no effective conditioning of the airflow noticed within the frontal part of chimp nasal vestibule. In chimpanzee, the air-conditioning occurred in the central nasal passages. This difference between both species in terms of nasal air-conditioning is attributed to the difference in the geometry of both nasal cavities, specifically the nostrils orientation.

Indeed, the ascending nostrils of human were coupled with the nasal cavity adjacent to its floor (Losken, et al., 1994) so the distance from nostrils tip to the anterior margin of the turbinates is short. In contrast to chimpanzee, which possess relatively long horizontal nostrils making the delay to condition the inhaled air. We attribute this to the fact that the long horizontal nostrils of chimpanzee are not mucous lined airways that are highly vascular to provide an ease exchange for heat and water transfer with the inspiratory flow stream. In contrast, their "luminal surface is lined by a squamous epithelium similar to that of external skin" (Harkema, et al., 2012).

CONCLUSION

Familiarity with chimpanzee nasal topology, airflow patterns, and air-conditioning structures is a source of knowledge to understand chimpanzee's nasal physiology and pathology. This fact could potentially contribute in accumulating standardized biological information on healthy chimpanzees, and so increasing the ability to care for them as endangered species. It would also support scientists interested in comparative biomedicine filed.

8.1 The anatomy of chimpanzee nasal cavity

This research work investigated the anatomy and airflow characteristics of chimpanzee nasal cavity. Computed tomography (CT) scanning of the head of a healthy adult female chimpanzee were used to reconstruct an anatomically-realistic model of the animal's nasal airways. An accurate three-dimensional (3D) computational fluid dynamics (CFD) model of the chimpanzee nasal topology was created, and results of airflow features were demonstrated.

8.2 Airflow in chimpanzee nasal cavity

1. Laminar steady airflow state of physiologically-correct breathing rate was investigated to reveal the flow patterns inside the chimpanzee nasal cavity during rest phase. Airflow patterns

2. included streamlined flow through the central nasal passage, and secondary flow (vortices) in the anterior margin of the nasal vestibule (nasopalatine duct region), due to the increasing in the cross-sectional area next to the nasal valve region; and in the dorsal upper paths diverting high velocity streams far away the olfactory site to prevent its damage.

3. The vestibule of the chimpanzee nasal passage operates as a laminar-flow streamliner for inspiratory air at rest state. The inhaled air, passing thru the relatively long and horizontal nostrils, continues flowing straight forward without bending, prior to splitting into peripheral, ventral, upper, and middle flow paths.

4. Outcomes of simulations showed that the airflow in the chimpanzee nasal cavity is mainly straight forward streamlined from the anterior margin of the vestibule till reaching nasopharyngeal region. Airflow patterns are affected by the internal features of the nasal topology such as the increasing of the cross-sectional area after the nasal valve region which produced a vortex inside the nasopalatine duct, the protrusion of conchae which generated narrow channels that streamlined the flow, the horizontally-oriented vestibule and nasopharynx kept the air flowing straight forward without bending.

8.3 Air-conditioning in chimpanzee nasal cavity

1. The general outline of the chimpanzee nasal topology was demonstrated to be in favor of effective air-conditioning.

2. The behavior of air-conditioning function inside chimpanzee nasal cavity was shown to vary according to sagittal and transverse sites.

3. The patterns in the lower, middle, and upper airways differ according to the nasal lining existing in those zones.

4. The air-conditioning distributions were shown to be independent of the nasal cavity side (left or right).

8.4 Future work

As future work, this model would serve to construct artificial nasal mold, which may validate CFD outcomes, demonstrated in this work, by means of experimental measurements.

REFERENCES

Becker, R. F. and King, J. E.: "Delineation of the Nasal Air Streams in the Living Dog," AMA Arch. Otolaryngol., **65**(5), pp. 428-436 (1957).

F. Bojsen-Moller and J. Fahrenkrug: "Nasal swell bodies and cyclic changes in the air passages of the rat and rabbit nose", J. Anat. 110, pp.25-37 (1971).

Bonn, D., Rodts, S., Groenink, M., Rafai, S., Shahidzadeh-Bonn, N., and Coussot, P.: "Some Applications of Magnetic Resonance Imaging in Fluid Mechanics: Complex Flows and Complex Fluids," Annu. Rev. Fluid Mech., **40**, pp. 209-233 (2008).

Corley, R. A., Minard, K. R., Kabilan, S., Einstein, D. R. and Kupart, A. P.: "Magnetic resonance imaging and computational fluid dynamics (CFD) simulations of rabbit nasal airflows for the development of hybrid CFD/PBPK models", Inhal Toxicol 21 (6), pp.512-518 (2009).

Dawes, J. D. K.: "The Course of the Nasal Airstreams," J. Laryngol. Otol., **66**(12), pp. 583-593 (1952).

De Rycke, L. M., Saunders, J. H., Gielen, I. M., van Bree, H. J., and Simoens, P. J.: "Magnetic Resonance Imaging, Computed Tomography, and Cross-Sectional Views of the Anatomy of Normal Nasal Cavities and Paranasal Sinuses in Mesaticephalic Dogs," American Journal of Veterinary Research, **64**(9), pp. 1093-1098 (2003).

R. Eccles and H. Wilson: "The autonomic innervation of the nasal blood vessels of the cat". J. Physiol. 238, pp.549-560 (1974).

R. Eccles: "The domestic pig as an experimental animal for studies on the nasal cycle", Acta Otolaryngol (Stockh) 85, pp.431-436 (1978).

R. Eccles and K. S. J. Eccles: "Sympathetic innervation of the nasal mucosa of the pig". Res Vet Sci. 30, pp.349-352 (1981).

Elkins, C. J., Markl, M., Pelc, N., and Eaton, J. K.: "4D Magnetic Resonance Velocimetry for Mean Velocity Measurements in Complex Turbulent Flows," Experiments in Fluids, **34**(4), pp. 494-503 (2003).

Elkins, C. J. and Alley, M. T.: "Magnetic Resonance Velocimetry: Applications of Magnetic Resonance Imaging in the Measurement of Fluid Motion," Experiments in Fluids, **43**(6), pp. 823-858 (2007).

R. N. T. W. Fiennes and E. K. Dzhikidze: "Respiratory pathoens and other organisms", In R. NT.-W. -Fiennes (Ed.), Pathology of Simian Primates, Basel: Karger, Part2, pp.277-282 (1972a).

R. N. T. W. Fiennes, B. A. Lapin, E. K. Dzhikidze and L. A. Yakovleva: "The respiratory and alimentary systems", In R. NT.-W. -Fiennes (Ed.), Pathology of Simian Primates, Basel: Karger, Part1, pp.671-710 (1972b).

Gagneux P., Moore J. J., and Varki A.:" The ethics of research on great apes", Nature 437(7055), pp.27-29 (2005).

Gross, E. A., Swenberg, J. A., Fields, S., and Popp, J. A.: "Comparative Morphometry of the Nasal Cavity in Rats and Mice," J. Anat., **135**(AUG), pp. 83-88 (1982).

Hahn, I., P.W. Scherer and M.M. Mozell.: "Velocity profiles measured for airflow through a large-scale model of the human nasal cavity." J Appl. Physiol. 75(5):2273-2287 (1993).

S.Hanida, F.Mori, K.Kumahata, M.Watanabe, S.Ishikawa and T.Matsuzawa: "Airflow Simulation of Nasal Cavity with Maxillary Sinus using Latent Heat Model" Proceeding of 10th International Symposium Computer Methods in Biomechanics and Biomedical Engineering pp.480-485 (2013).

Harkema, Jack R., Carey, Stephan A., Wagner, James G., Dintzis, Suzanne M., and Liggitt Denney: "Nose, Sinus, Pharynx, and Larynx" Comparative Anatomy and Histology: A Mouse and Human Atlas edited by Piper M. Treuting, Suzanne M. Dintzis, Charles W. Frevert, H. Denny Liggitt, Kathleen S. Montine, Chap. 6, 2012.

Harris, A. J., Squires, S. M., Hockings, P. D., Campbell, S. P., Greenhill, R. W., Mould, A., and Reid, D. G.: "Determination of Surface Areas, Volumes, and Lengths of Cynomolgus Monkey Nasal Cavities by Ex Vivo Magnetic Resonance Imaging," Journal of Aerosol Medicine-Deposition Clearance and Effects in the Lung, 16(2), pp. 99-105 (2003).

H. Hofer: "Preliminary study of the comparative anatomy of the external nose of South American monkeys", Folia Primatol. 25, pp.193-214 (1976).

Hopkins, L. M., Kelly, J. T., Wexler, A. S., and Prasad, A. K.: "Particle Image Velocimetry Measurements in Complex Geometries," Experiments in Fluids, **29**(1), pp. 91-95 (2000).

D. E. Hornung and M. M. Mozell: "Accessibility of odorant molecules to the receptors". In Cagan, R.H. and Kare, M.R. (eds), Biochemistry of Taste and Olfaction. Academic Press, New York, pp.33-45 (1981).

Hornung, D. E., Leopold, D. A., Youngentob, S. L., Sheehe, P. R., Gagne, G. M., Thomas, F. D., and Mozell, M. M.: "Airflow Patterns in a Human Nasal Model," Arch. Otolaryngol. Head Neck Surg., **113**(2), pp. 169-172 (1987).

E. L. House, B. Pansky, M. S. Jacobs, and B. M. Wagner. Gross structure of the ear, nasal cavity and paranasal sinuses of the Chimpanzee. Anatomical Record, 155(1):77-88, 1966.

Roger Jankowski: "Olfactory and Respiratory Nasal Fossae", Chapter in *The Evo-Devo Origin of the Nose, Anterior Skull Base and Midface,* Springer pp.79-87 (2012).

Kaur, T. and Singh, J.: "Disease Transmission, Ecosystems Health and Great Apes Research", American Journal of Primatology (2008).

J. T. Kelly, A. K. Prasad, A. S. Wexler: 'Detailed flow patterns in the nasal cavity', Journal of Applied Physiology, Vol. 89 no. 1 (2000), pp.323-337.

Kepler, G. M., Richardson, R. B., Morgan, K. T., and Kimbell, J. S.: "Computer Simulation of Inspiratory Nasal Airflow and Inhaled Gas Uptake in a Rhesus Monkey," Toxicol. Appl. Pharmacol., 150(1), pp. 1-11 (1998).

Keyhani, K., Scherer, P. W., and Mozell, M. M.: "Numerical Simulation of Airflow in the Human Nasal Cavity," Journal of Biomechanical Engineering-Transactions of the Asme, **117**(4), pp. 429-441 (1995).

Keyhani, K., Scherer, P. W., and Mozell, M. M.: "A Numerical Model of Nasal Odorant Transport for the Analysis of Human Olfaction," J. Theor. Biol., **186**(3), pp. 279-301 (1997).

Kimbell, J. S., Gross, E. A., Joyner, D. R., Godo, M. N., and Morgan, K. T.: "Application of Computational Fluid Dynamics to Regional Dosimetery of Inhaled Chemicals in the Upper Respiratory Tract of the Rat," Toxicol. Appl. Pharmacol., **121**(2), pp. 253-263 (1993).

Kimbell, J. S., Godo, M. N., Gross, E. A., Joyner, D. R., Richardson, R. B., and Morgan, K. T.: "Computer Simulation of Inspiratory Airflow in All Regions of the F344 Rat Nasal Passages," Toxicol. Appl. Pharmacol., **145**(2), pp. 388-398 (1997).

Kimbell, J. S., Subramaniam, R. P., Gross, E. A., Schlosser, P. M., and Morgan, K. T.: "Dosimetry Modeling of Inhaled Formaldehyde: Comparisons of Local Flux Predictions in the Rat, Monkey, and Human Nasal Passages," Toxicological Sciences, **64**(1), pp. 100-110 (2001).

Kumahata K, Mori F, Ishikawa S, Matsuzawa T: "Nasal flow simulation using heat and humidity models". *J Biomech Sci Eng* 5:565‑577 (2010).

B. A. Lapin and L. A. Yakovleva: "In Comparative Pathology in Monkeys", Springfield, IL: Thomas (1963).

Lee, C. Y. and Wilke, C. R., Measurements of vapor diffusion coefficient, Industrial and Engineering Chemistry 46, 11 (1954), pp.2381 –2387.

Leonard, B.P. and S. Mokhtari.: "ULTRA-SHARP Nonoscillatory convection schemes for high-speed steady multidimensional flow." NASA Lewis Research Center (1990).

Anders Lervik, Fernando Bresme, Signe Kjelstrup, Dick Bedeaux and J. Miguel Rubi.: 'Heat transfer in protein–water interfaces', Phys. Chem. Chem. Phys., 2010, 12, 1610-1617.

Lindemann, J., Keck, T., Wiesmiller, K., Sander, L., Brambs, H. J., Rettinger, G., and Pless, D.: "A Numerical Simulation of Intranasal Air Temperature during Inspiration," Laryngoscope, **114**(6), pp. 1037-1041 (2004).

Lindemann, J., Keck, T., Wiesmiller, K., Sander, B., Brambs, H. J., Rettinger, G., and Pless, D.: "Nasal Air Temperature and Airflow During Respiration in Numerical Simulation Based on Multislice Computed Tomography Scan," American Journal of Rhinology, **20**(2), pp. 219-223 (2006).

Losken A, Mooney MP, and Siegel MI: "Comparative cephalometric study of nasal cavity growth patterns in seven animal models". *Cleft Palate Craniofac J* 31:17‑23 (1994).

L. J. Lowenstine: "A primer of primate pathology: lesions and non-lesions", Toxicologic Pathology, 31(suppl. 1), pp.1-11 (2003).

Marshall, I., Zhao, S. Z., Papathanasopoulou, P., Hoskins, P., and Xu, X. Y.: "MRI and CFD Studies of Pulsatile Flow in Healthy and Stenosed Carotid Bifurcation Models," Journal of Biomechanics, **37**(5), pp. 679-687 (2004).

D. P. Martin: "Primates", In M. E. Fowler (Ed.), Zoo and Wild Animal Medicine, Vol. 3, Philadelphia: Saunders, Curr. Ther., pp.525-552 (1978).

Matsuzawa, T., Tomonaga, M. and Tanaka, M.: "Cognitive development in chimpanzees" Springer (2006).

Menache, M. G., Hanna, L. M., Gross, E. A., Lou, S. R., Zinreich, S. J., Leopold, D. A., Jarabek, A. M., and Miller, F. J.: "Upper Respiratory Tract Surface Areas and Volumes of Laboratory Animals and Humans: Considerations for Dosimetry Models," Journal of Toxicology and Environmental Health, **50**(5), pp. 475-506 (1997).

Minard, K. R., Einstein, D. R., Jacob, R. E., Kabilan, S., Kuprat, A. P., Timchalk, C. A., Trease, L. L., and Corley, R. A.: "Application of Magnetic Resonance (MR) Imaging for the Development and Validation of Computational Fluid Dynamic (CFD) Models of the Rat Respiratory System," Inhal. Toxicol., **18**(10), pp. 787-794 (2006).

J. R. Minkel: "Humans and Chimps: Close But Not That Close", Scientific American (19 Dec. 2006).

Moore, S., David, T., Chase, J.G., Arnold, J., and Fink, J.: "3D models of blood flow in cerebral vasculature", Journal of Biomechanics (2005).

Morgan, K. T. and Monticello, T. M.: "Air-Flow, Gas Deposition, and Lesion Distribution in the Nasal Passages," Environmental Health Perspectives, **85**, pp. 209-218 (1990).

Morgan, K. T., Kimbell, J. S., Monticello, T. M., Patra, A. L., and Fleishman, A.: "Studies of Inspiratory Air-Flow Patterns in the Nasal Passages of the F344 Rat and Rhesus-Monkey Using Nasal Molds - Relevance to Formaldehyde Toxicity," Toxicol. Appl. Pharmacol., **110**(2), pp. 223-240 (1991).

Nishimura T, Mori F, Hanida S, Kumahata K, Ishikawa S, Samarat K, et al. (2016) Impaired Air Conditioning within the Nasal Cavity in Flat-Faced Homo . PLoS Comput Biol 12(3): e1004807.

Mori F, Hanida S, Kumahata K, Miyabe–Nishiwaki T, Suzuki J, Matsuzawa T, et al. Minor contributions of the maxillary sinus to the air-conditioning performance in macaque monkeys. J Exp Biol. 2015; 218: 2394–2401.

Tarjei S. Mikkelsen, LaDeana W. Hillier, Evan E. Eichler, et. al.,: "Initial sequence of the chimpanzee genome and comparison with the human genome", NATURE, Vol 437, pp. 69-87 (2005).

Oldham, M.J., Phalen, R.F. and Heistracher, T.: "Computational fluid dynamic predictions and experimental results for particle deposition in an airway model", Aerosol Science and technology 32(1), pp.61-71.

Patankar, S. V.: "Numerical Heat Transfer and Fluid Flow". *Taylor & Francis* (1980).

Patra, A. L., Gooya, A., and Morgan, K. T.: "Air-Flow Characteristics in A Baboon Nasal Passage Cast," J. Appl. Physiol., **61**(5), pp. 1959-1966 (1986).

Patra, A. L., Menache, M. G., Shaka, N. B., and Gooya, A.: "A Morphometric Study of Nasal-Pharyngeal Growth for Particle Deposition in the Rat," American Industrial Hygiene Association Journal, **48**(6), pp. 556-562 (1987).

Paulsen, E.: "Experimentelle Untersuchungen Über Die Strömungen Der Luft in Der Nasenhöhle," Sitzungsberichte der kaiserliche Academie der Wissenschaften, III Abteilung, **85**, pp. 348 (1882).

Pless, D., Keck, T., Wiesmiller, K., Rettinger, G., Aschoff, A. J., Fleiter, T. R., and Lindemann, J.: "Numerical Simulation of Air Temperature and Airflow Patterns in the Human Nose during Expiration," Clinical Otolaryngology, **29**(6), pp. 642-647 (2004).

Proetz, A. W.: "Air Currents in the Upper Respiratory Tract and Their Clinical Importance," Annals of Otology Rhinology and Laryngology, **60**(2), pp. 439-467 (1951).

Proetz, A. W.: "*Applied Physiology of the Nose*", Annals Publishing Co., St. Louis (1953).

N. V. Reo, J. K. C. Barnett, T. A. Neubecker, M. E. Alexander, C. M. Goecke: "A nuclear-magnetic-resonance investigation of the upper airways in ferrets. I. Effects of histamine and methacholine". Magn. Reson. Med. 27, pp.21-33 (1992).

Richmond, C.: "Sir Godfrey Hounsfield." British Medical Journal 329(7467) p.687 (2004).

Saber, N.R., Wood, N.B., Gosman, A.D., Merrifield, R.D., Yang, G.Z., Charrier, C., Gatehouse, P.D. and Firmin, D.N.: "Progress towards patient–specific computational flow modelling of the left heart via combination of magnetic resonance imaging with computational fluid dynamics", Annals of Biomedical Engineering 31(1), pp.42-52.

Schreck, S., K.J. Sullivan, C.M. Ho and Chang H.K.: "Correlations between flow resistance and geometry in a model of the human nose." J. Appl.Physiol 75(4):1767-1775 (1993).

Schreider, J. P. and Raabe, O. G.,: "Anatomy of the Nasal-Pharyngeal Airway of Experimental Animals," Anat. Rec., **200**, pp. 195-205 (1981).

Schreider, J. P.: "Nasal airway anatomy and inhalation deposition in experimental animals and people," in *Nasal tumors in animals and man*, pp. 1-36 (1983).

A. H. Schultz: "The nasal cartilages in higher primates", Am. J. Phys. Anthropol. 20, pp.205-212 (1935).

Simmen, D., Scherrer, J. L., Moe, K., and Heinz, B.: "A Dynamic and Direct Visualization Model for the Study of Nasal Airflow," Arch. Otolaryngol. Head Neck Surg., **125**(9), pp. 1015-1021 (1999).

Smith TD, Siegel MI, Bonar CJ, Bhatnagar KP, Mooney MP, Burrows AM, Smith MA, Maico LM: "The existence of the vomeronasal organ in postnatal chimpanzees and evidence for its homology with that of humans." J. Anat. 198 pp. 77-82 (2001).

Stahl, W. R.: "Scaling of respiratory variables in mammals", J. Appl. Physiol. 22, pp.453-460 (1967).

Stitzel, S. E., Stein, D. R., and Walt, D. R.: "Enhancing Vapor Sensor Discrimination by Mimicking a Canine Nasal Cavity Flow Environment," Journal of the American Chemical Society, **125**(13), pp. 3684-3685 (2003).

Subramaniam, R. P., Richardson, R. B., Morgan, K. T., Kimbell, J. S., and Guilmette, R. A.: "Computational Fluid Dynamics Simulations of Inspiratory Airflow in the Human Nose and Nasopharynx," Inhal. Toxicol., **10**(5), pp. 473-502 (1998).

Swift, D. L. and Proctor, D. F.: "Access of Air to the Respiratory Tract," in *Respiratory Defense Mechanisms*, Chap. 3 (1977).

Tang, Z.H., Sheng, L.X., Parsons, S. et al.: "Fruit-feeding behaviour and use of olfactory cues by the fruit batRousettus leschenaulti: an experimental study", Acta Theriol (2007) 52: 285.

Taylor, C. A. and Draney, M. T.: "Experimental and Computational Methods in Cardiovascular Fluid Mechanics," Annu. Rev. Fluid Mech., **36**, pp. 197-231 (2004).

Timchalk, C., Trease, H. E., Trease, L. L., Minard, K. R., and Corley, R. A.: "Potential Technology for Studying Dosimetry and Response to Airborne Chemical and Biological Pollutants," Toxicology and Industrial Health, **17**(5-10), pp. 270-276 (2001).

Vandoormaal, J.P. and G.D. Raithby.: "Enhancements of the SIMPLE method for predicting incompressible fluid flows." Numer. Heat Transfer 7 pp.147-163 (1984).

Vennemann, P., Lindken, R., and Westerweel, J.: "In Vivo Whole-Field Blood Velocity Measurement Techniques," Experiments in Fluids, **42**(4), pp. 495-511 (2007).

J. D. Wallach and W. J. Boever: "Primates", In: Diseases of Exotic Animals. Medical and Surgical Management. Philadelphia: Saunders, pp.1-133 (1983).

R. L. Webber, M. K. Jeffcoat, J. T. Harman, U. E. Ruttimann: "MR demonstration of the nasal cycle in the beagle dog". J Comput. Assist. Tomogr. 11, pp.869-871 (1987).

Weibel, E. R.: '*Morphometry of the Human Lung",* Academic Press., New York, US (1963).

I. C. Wen: "Ontogeny and phylogeny of the nasal cartilages in primates", Contrib. Embryol. 130, 111-134 (1930).

Vogel, S.: "Life in Moving Fluids" Princeton Univ. Press, Princeton, N.J (1994).

Worthington, J., Young, I. S. and Altringham, J. D.: "The relationship between body-mass and ventilation rate in mammals", J. Exp. Biol. 161, pp.533-536 (1991).

Xu, C., Sin, S.H., McDonough, J.M., Udupa, J.K., Guez, A., Arens, R. and Wootton, D.M.: "Computational fluid dynamics modelling of the upper airway of children with obstructive sleep apnea syndrome in steady flow", Journal of Biomechanics 39(11), pp.2043-2054.

Yeh, H. C., Brinker, R. M., Harkema, J. R., and Muggenburg, B. A.: "A Comparative Analysis of Primate Nasal Airways Using Magnetic Resonance Imaging and Nasal Casts," Journal of Aerosol Medicine-Deposition Clearance and Effects in the Lung, 10(4), pp. 319-329 (1997).

Zhao, K., Scherer, P. W., Hajiloo, S. A., and Dalton, P.: "Effect of Anatomy on Human Nasal Air Flow and Odorant Transport Patterns: Implications for Olfaction," Chem. Senses, **29**(5), pp. 365-379 (2004).

Zhao, K., Dalton, P., Yang, G. C., and Scherer, P. W.: "Numerical Modeling of Turbulent and Laminar Airflow and Odorant Transport During Sniffing in the Human and Rat Nose," Chem. Senses, **31**(2), pp. 107-118 (2006).

S J Zinreich, D W Kennedy, J Malat, H D Curtin, J I Epstein, L C Huff, A J Kumar, M E Johns, and A E Rosenbaum: "Fungal sinusitis: diagnosis with CT and MR imaging.", Radiology 169 (2) 1988.

Jian Hua Zhu, Heow Pueh Lee, Kian Meng Lim, Shu Jin Lee, and De Yun Wang: "Evaluation and comparison of nasal airway flow patterns among three subjects from Caucasian, Chinese and Indian ethnic groups using computational fluid dynamics simulation", Respiratory Physiology & Neurobiology 175(1), 2011, pp. 62-69.

APPENDIX I

Figure A.1. CT scans of the chimpanzee head spanned from the anterior of the larynx to the mouth tip

Figure A.2: CT scans of the chimpanzee head (cont.)

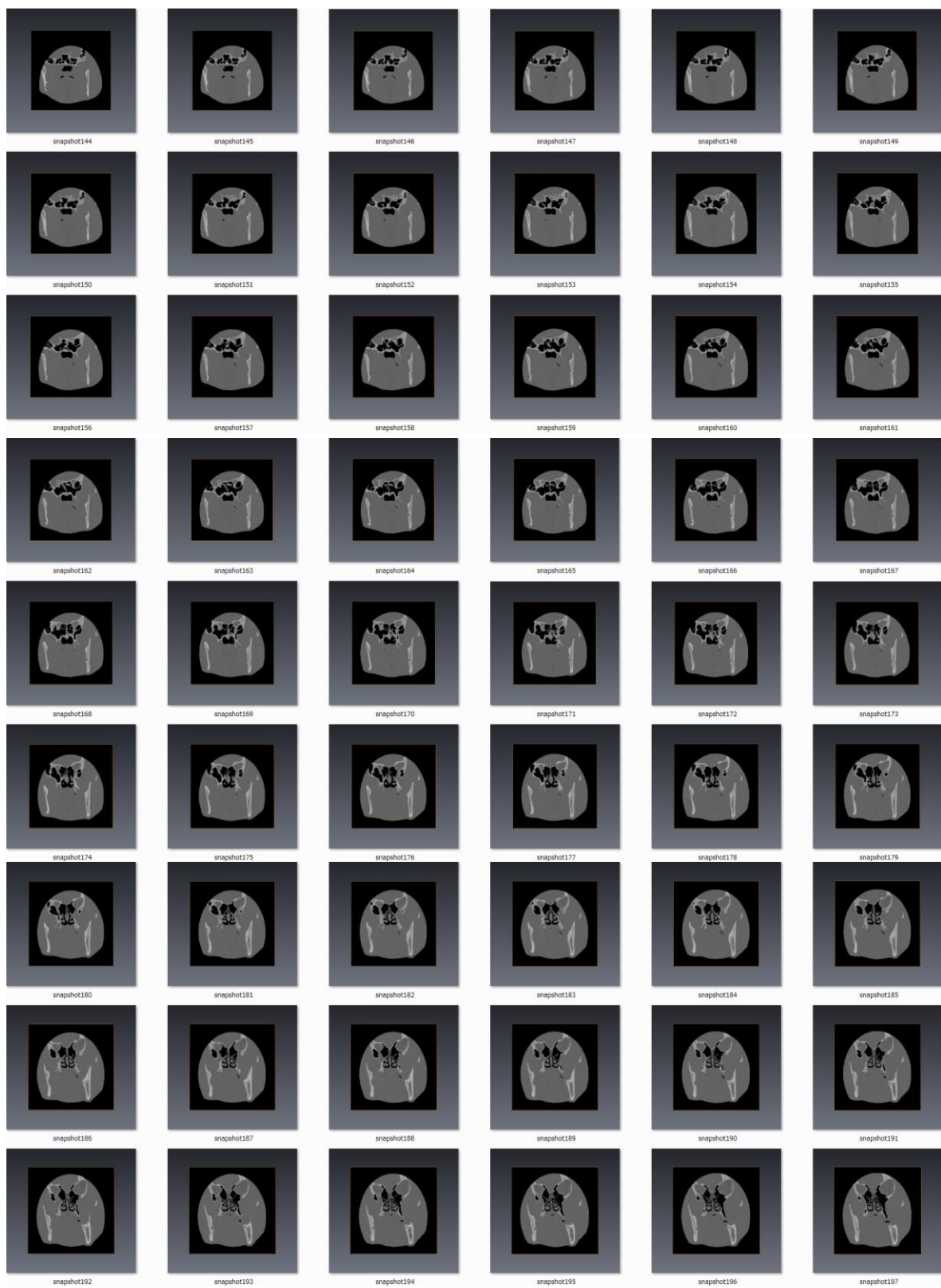Figure A.2: CT scans of the chimpanzee head (cont.).

Figure A.2: CT scans of the chimpanzee head (cont.)

CT scans of the chimpanzee head (cont.)

Figure A.2: CT scans of the chimpanzee head (cont.)

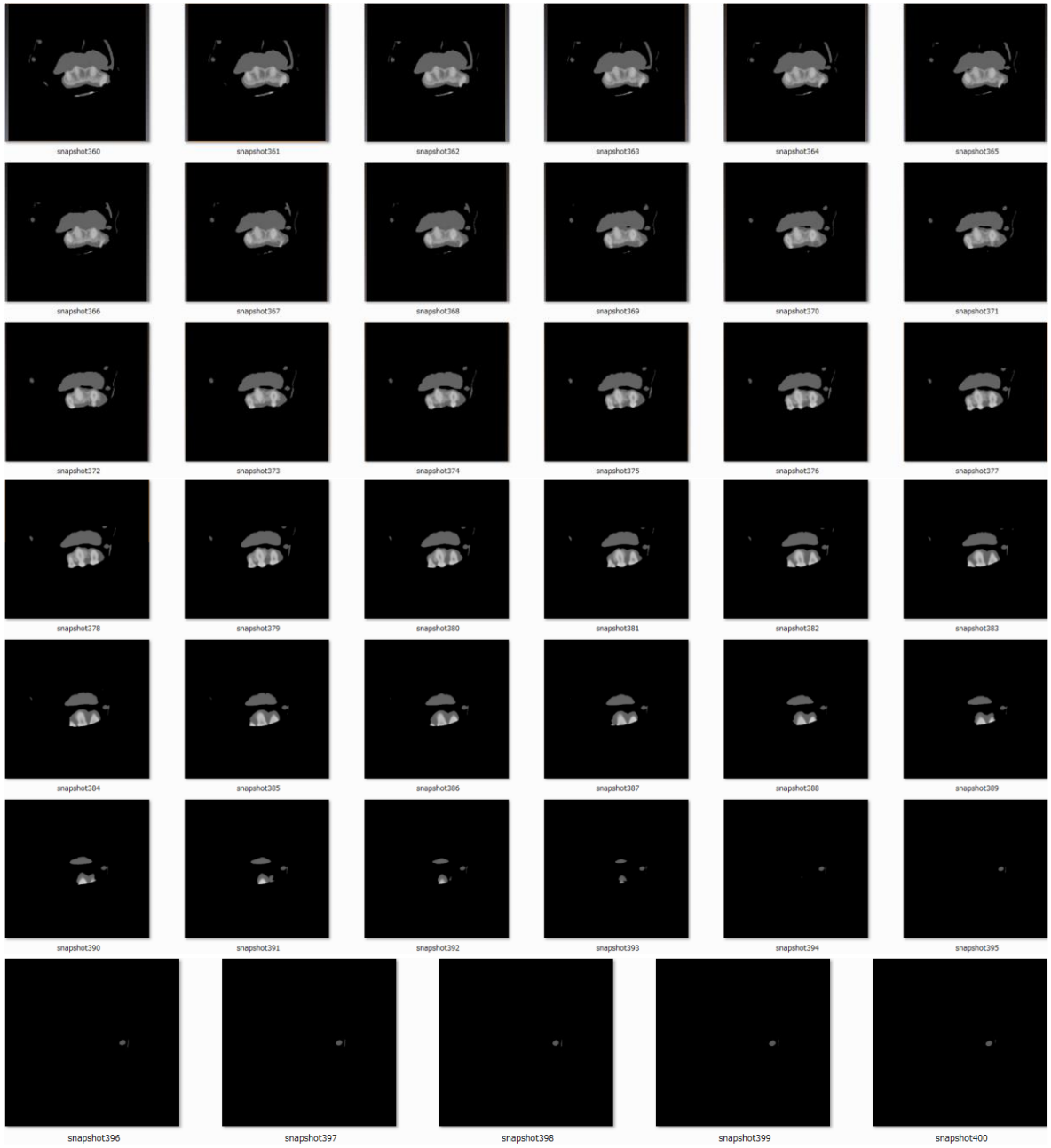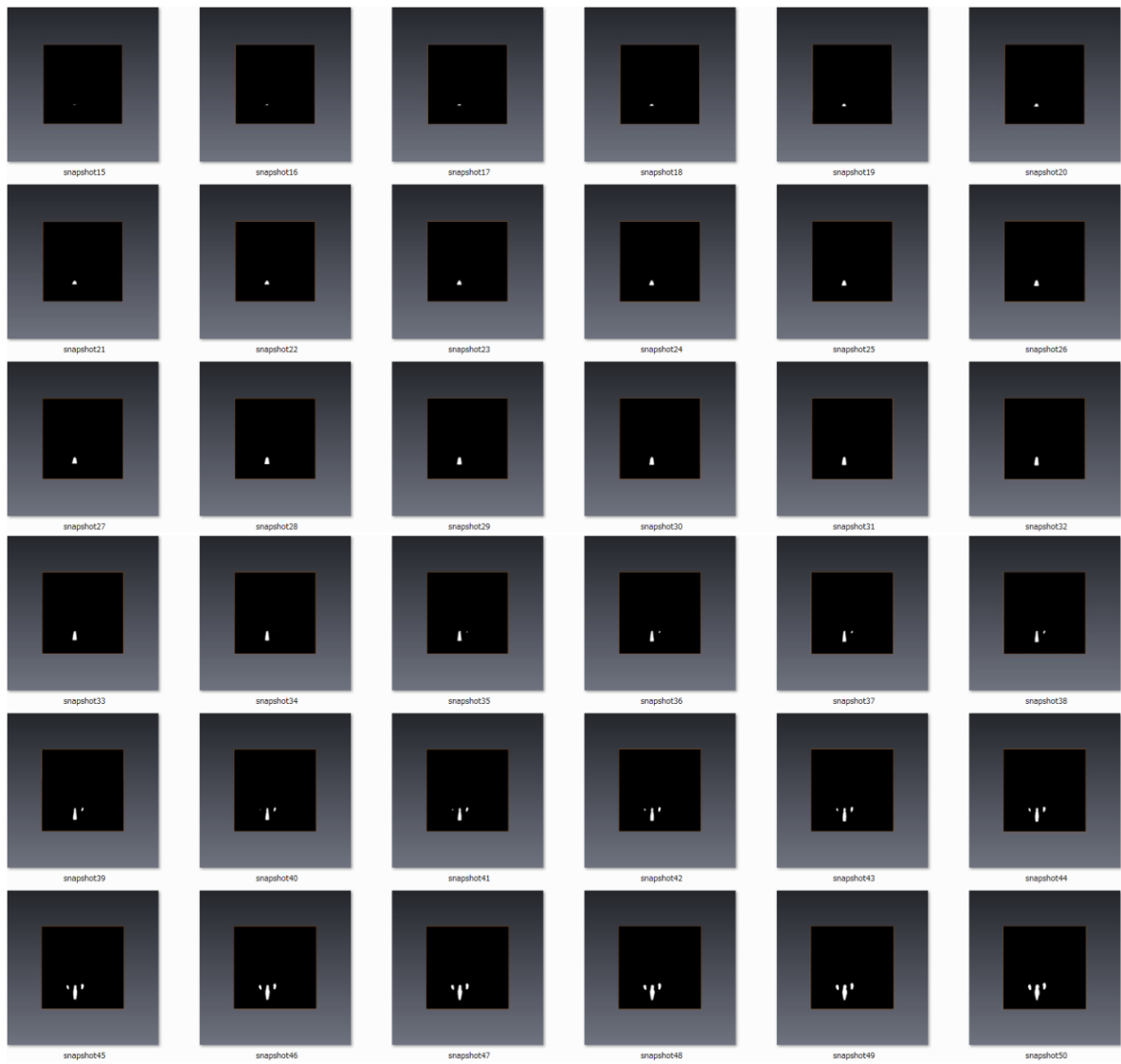Figure A.2: CT scans of the chimpanzee head (cont.)

Figure A.2: CT scans of the chimpanzee head

APPENDIX II

Figure A.2. Sub-image creation: Extraction of the chimpanzee nasal airway from the original CT scans of the head
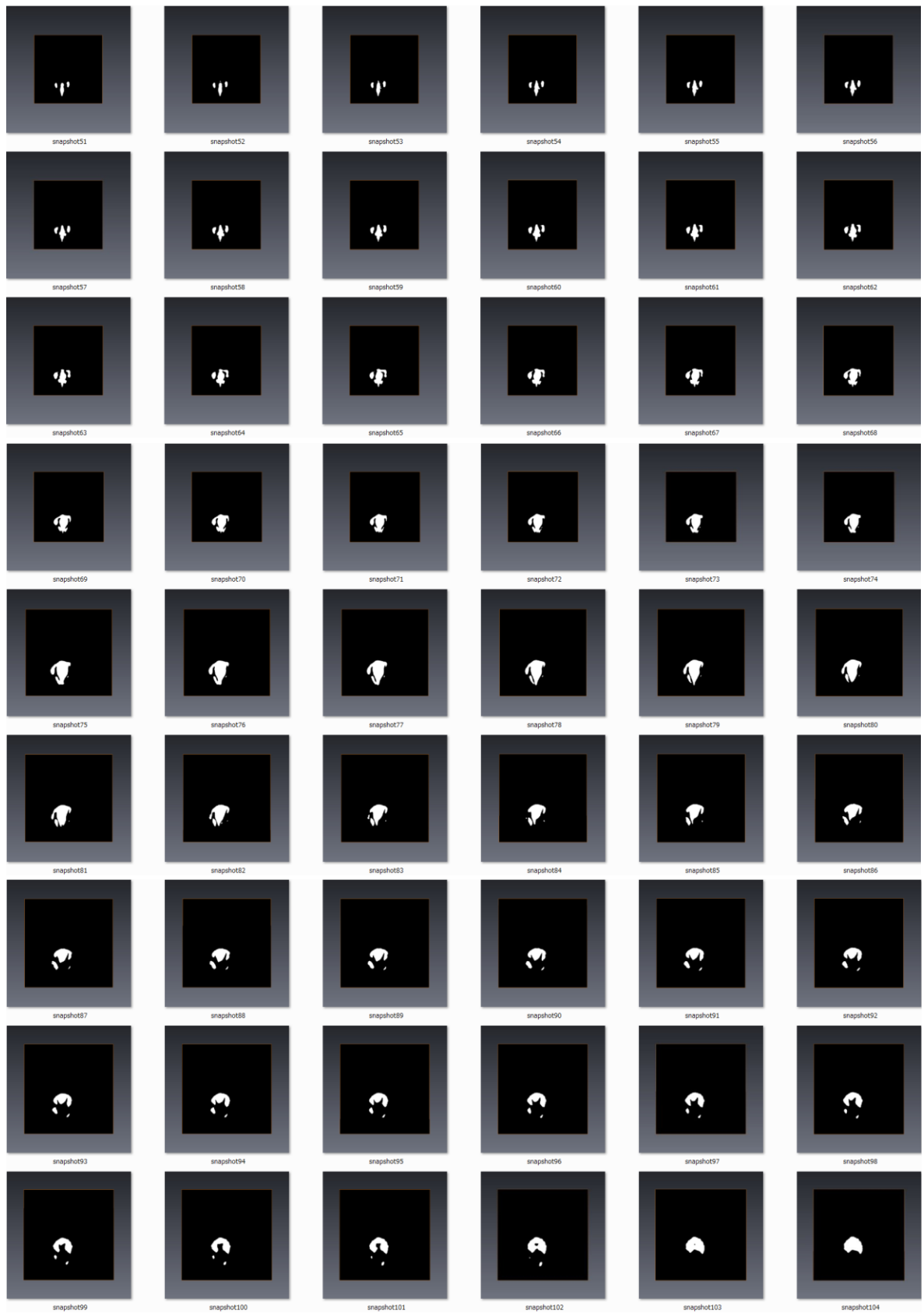
Figure A.3. Sub-image creation: Extraction of the chimpanzee nasal airway from the original CT scans of the head *(cont.)*
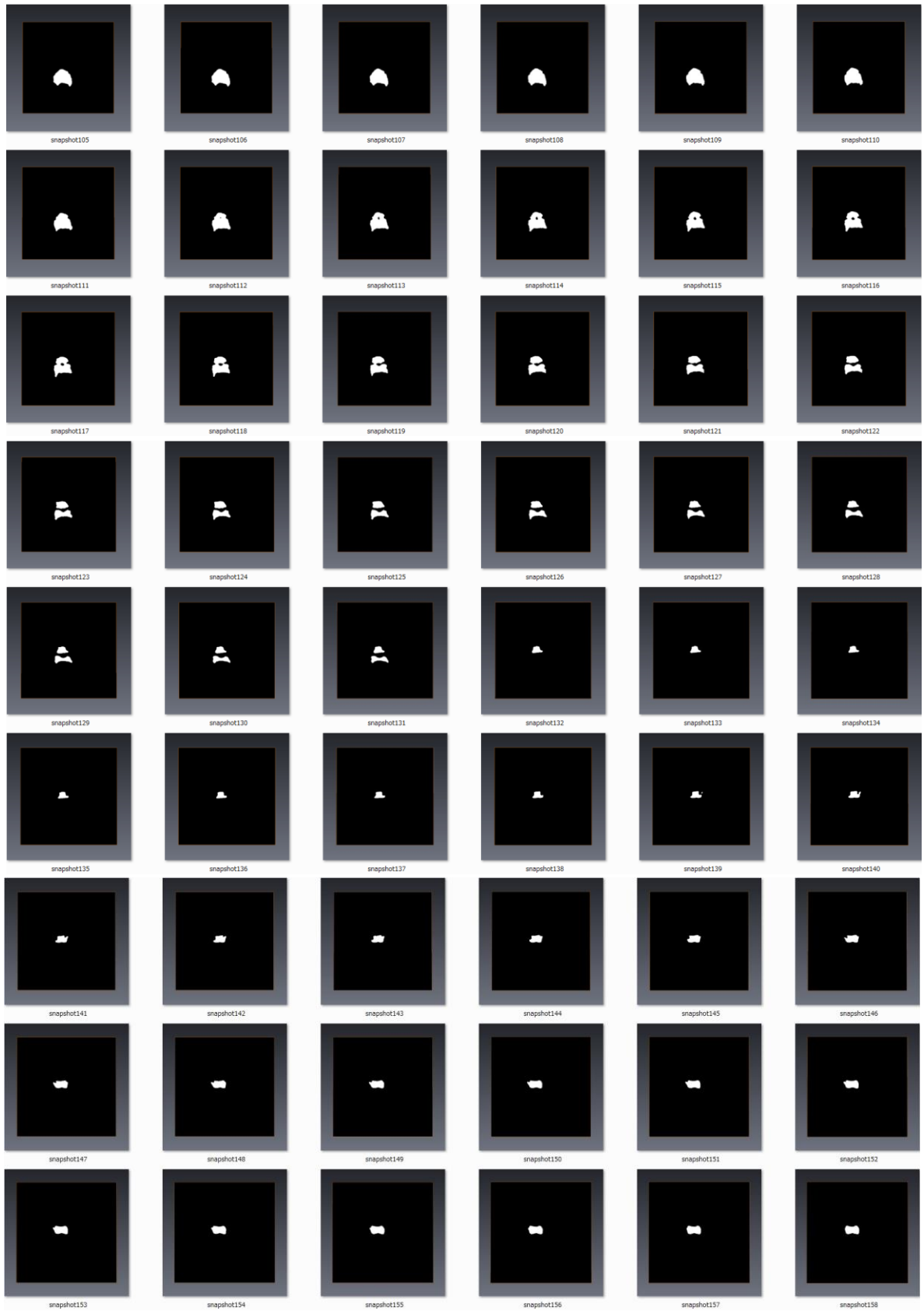
snapshot105 snapshot106 snapshot107 snapshot108 snapshot109 snapshot110

snapshot111 snapshot112 snapshot113 snapshot114 snapshot115 snapshot116

snapshot117 snapshot118 snapshot119 snapshot120 snapshot121 snapshot122

snapshot123 snapshot124 snapshot125 snapshot126 snapshot127 snapshot128

snapshot129 snapshot130 snapshot131 snapshot132 snapshot133 snapshot134

snapshot135 snapshot136 snapshot137 snapshot138 snapshot139 snapshot140

snapshot141 snapshot142 snapshot143 snapshot144 snapshot145 snapshot146

snapshot147 snapshot148 snapshot149 snapshot150 snapshot151 snapshot152

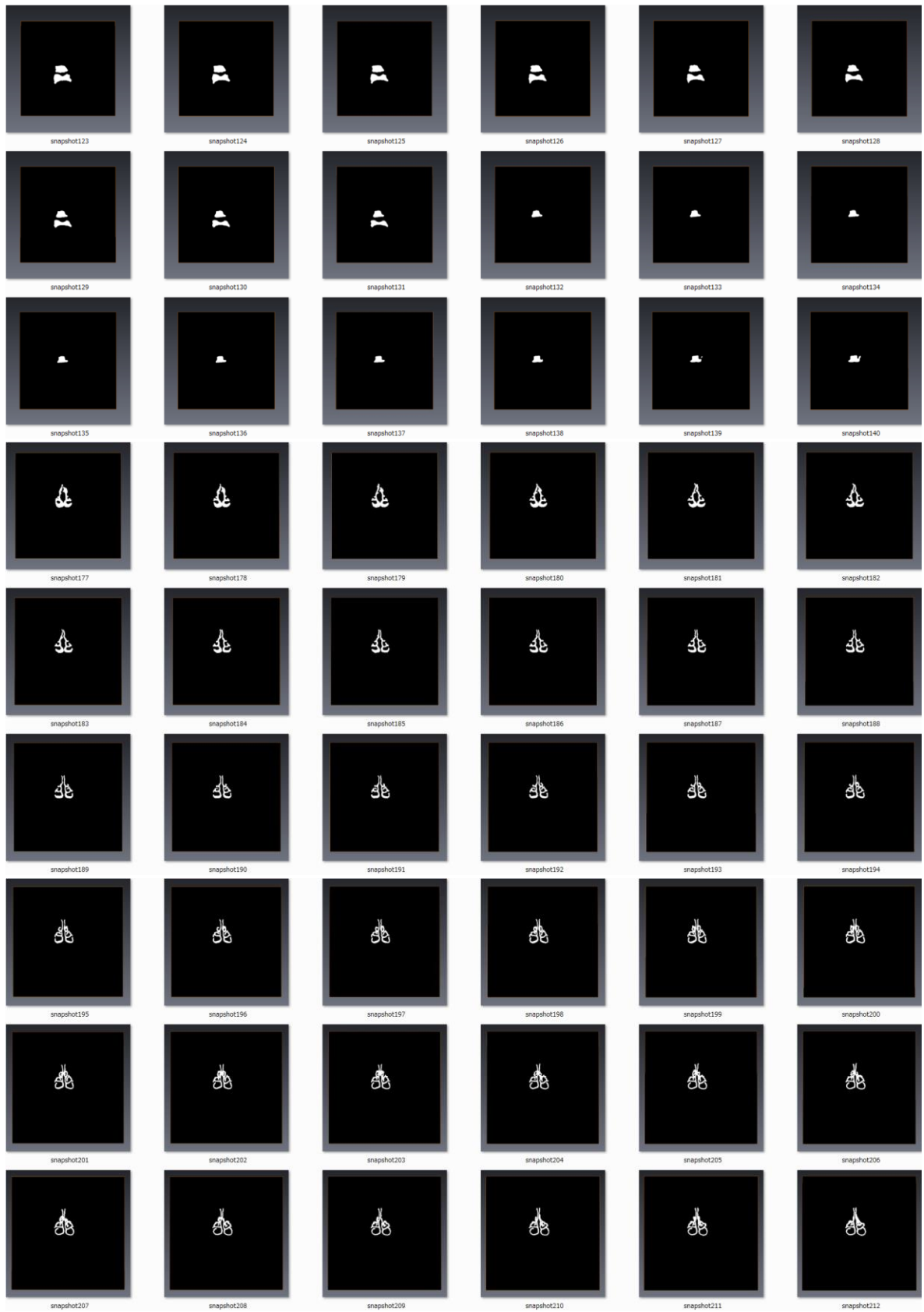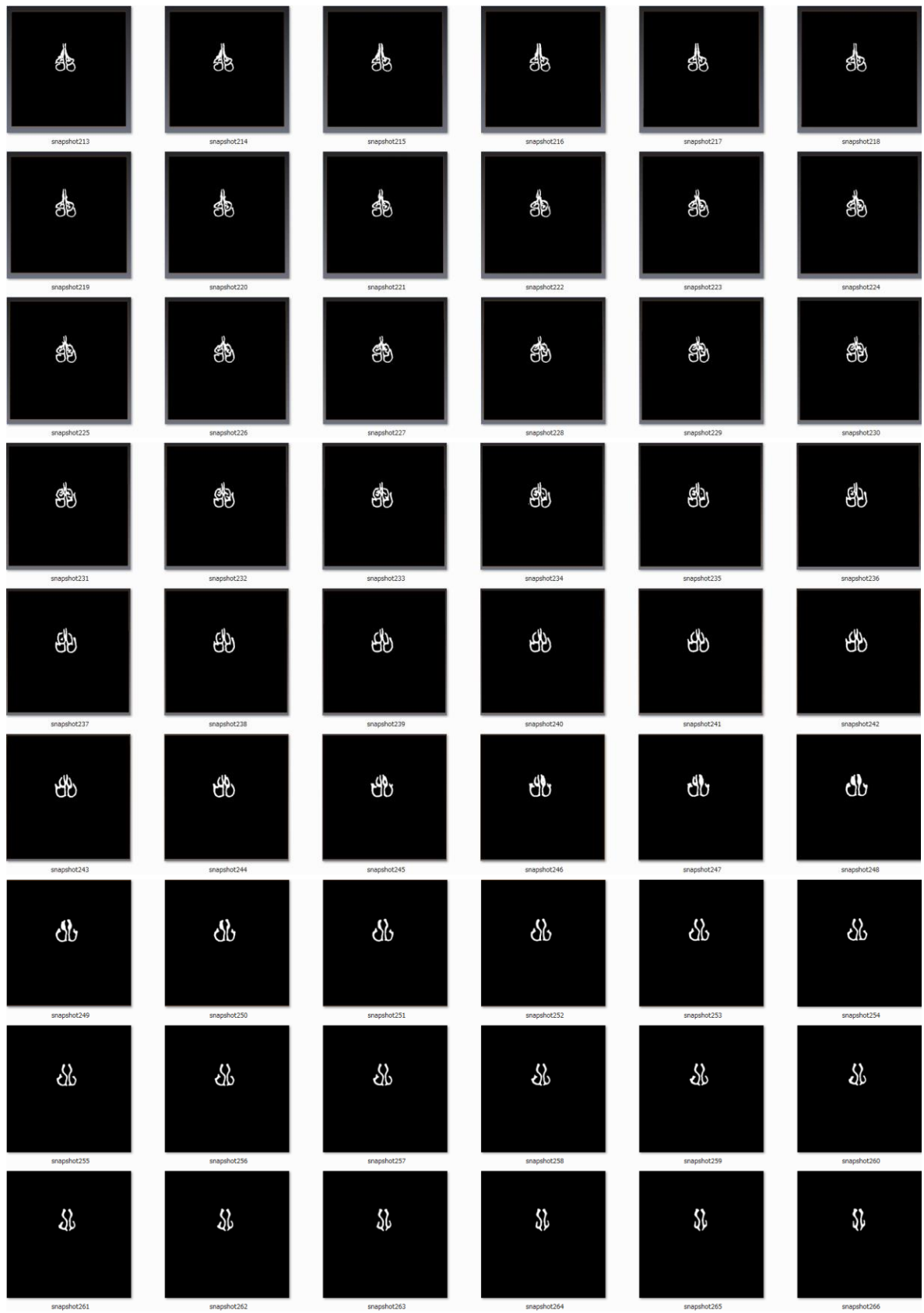snapshot153 snapshot154 snapshot155 snapshot156 snapshot157 snapshot158

Figure A.3. Sub-image creation: Extraction of the chimpanzee nasal airway from the original CT scans of the head *(cont.)*

Figure A.3. Sub-image creation: Extraction of the chimpanzee nasal airway from the original CT scans of the head *(cont.)*
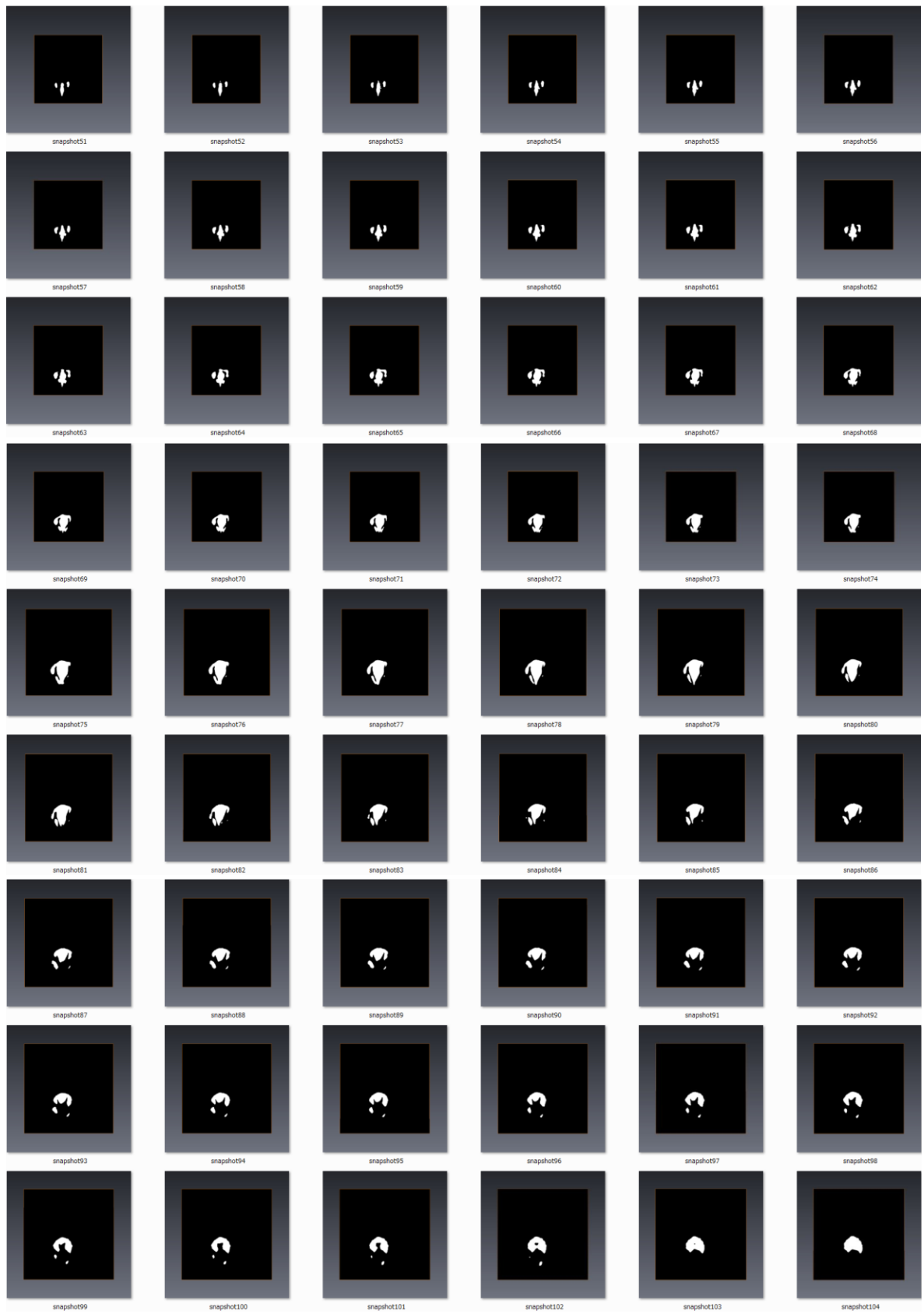
Figure A.3. Sub-image creation: Extraction of the chimpanzee nasal airway from the original CT scans of the head *(cont.)*

Figure A.3. Sub-image creation: Extraction of the chimpanzee nasal airway from the original CT scans of the head *(cont.)*
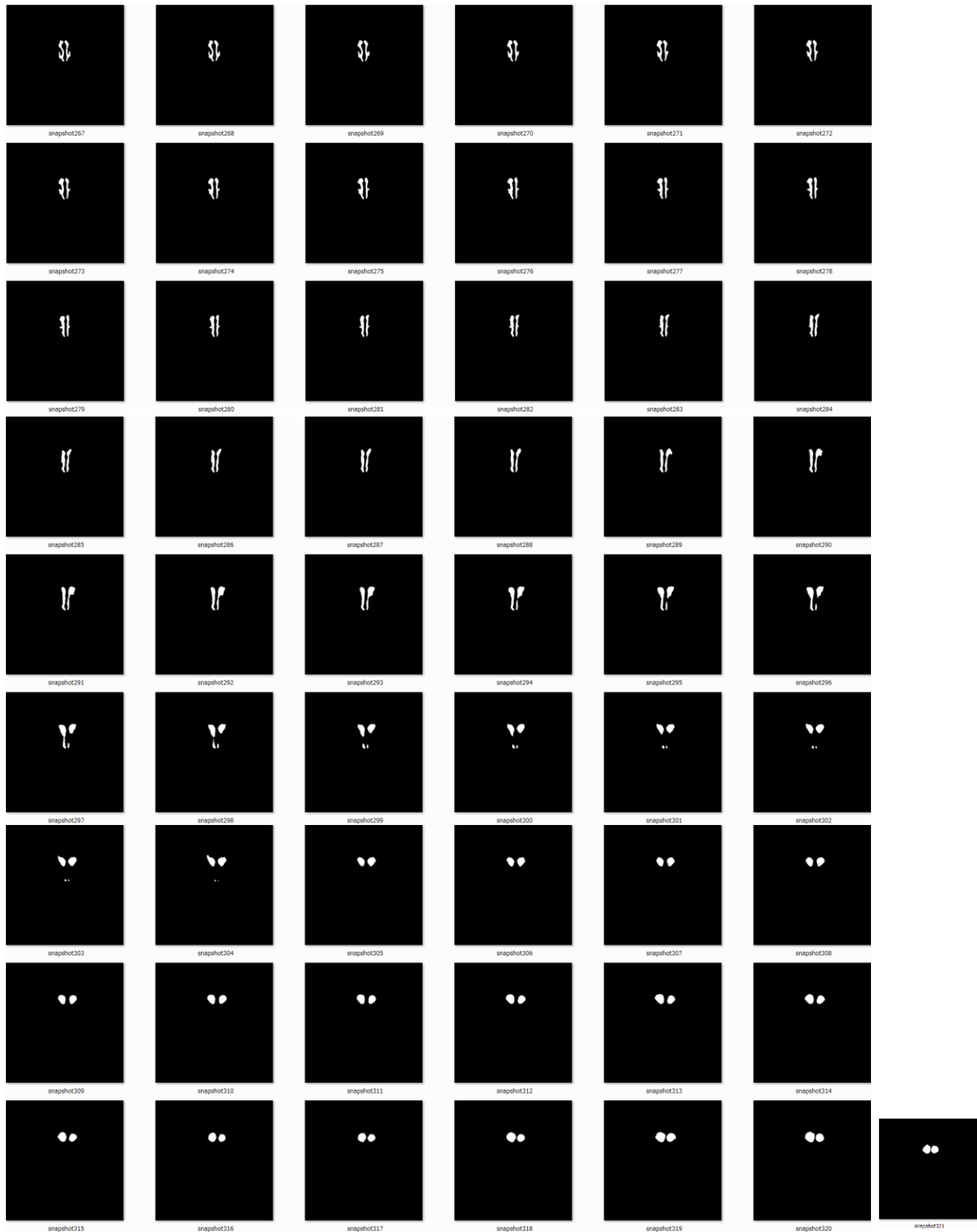
Figure A.3. Sub-image creation: Extraction of the chimpanzee nasal airway from the original CT scans of the head.

LIST OF PUBLICATIONS

Refereed Journal Article

Samarat, K., and Matsuzawa, T., "A Computational Model of the Anatomy of Realistic Chimpanzee Nasal Airways", *IJIR*, 2 (2) pp.357-364 (2016). [IF: 3.75]

International Conference

Samarat, K., Kotani, K. and Matsuzawa, T.: "Nasal air-conditioning in chimpanzee".
28th International Conference on Parallel Computational Fluid Dynamics (Parallel CFD 2016), Kobe, Japan, May 9-12, 2016 (Oral presentation).

Samarat, K., Kumahata, K., Hanida, S., Nishimura, T., Mori, F., Ishikawa, S., and Matsuzawa, T., "Application of Computational Fluid Dynamics to Simulate a Steady Airflow in All Regions of Chimpanzee's Nasal Cavity", in Procedia Engineering (61) 2013, pages 264–269, *25th International Conference on Parallel Computational Fluid Dynamics (ParCFD 2013)*, Changsha, China, May 20-24, 2013.